Arch. Mech., 49, 3, pp. 477–511, Warszawa 1997

Viscoplastic shells
Theory and numerical analysis (1)

Dedicated to Professor Franz Ziegler
on the occasion of His 60th birthday

F.G. KOLLMANN and C. SANSOUR (DARMSTADT)

THE PAPER is intended as a review of the work carried out at the institute to which the authors belong, regarding the theory of viscoplastic shells in both versions of small and finite strains. Within the first version, the kinematics incorporated is assumed to be linear allowing for an additive decomposition of the strain rate. For the axisymmetric case, a hybrid strain-based functional is presented. Contrasting this, in the finite strain case, the shell kinematics is considered as geometrically exact. Here, the shell theory itself is seven-parametric and allows for the application of a three-dimensional constitutive law. The constitutive law used is that of Bodner & Partom which falls within the class of unified constitutive models. The multiplicative decomposition of the deformation gradient is employed, but no use is made of the so-called intermediate configuration. The elastic constitutive law is of a logarithmic type. An enhanced strain finite element formulation is developed and several examples of finite deformations of various shell geometries are presented.

1. Introduction

MANY TECHNICALLY important structures can be modelled as shells, i.e. as curved bodies where one dimension, which is called the thickness, is much smaller than its other dimensions. In some applications, the material behaviour of metallic shells can be modelled by viscoplastic constitutive equations which describe rate-dependent deformation behaviour. Despite their technical importance, not so many publications deal with viscoplastic shells. In this paper we will present an overview on the work carried out at the institute to which the authors belong with regard to viscoplastic shells and their numerical analysis.

The paper will be split into two parts. In the first part we will briefly discuss a general, but geometrically linear theory of viscoplastic shells. The viscoplastic deformation behaviour can be governed by any of the more recently published so-called unified models with internal variables. Furthermore, we will demonstrate the application of the shell theory to the formulation of a family of mixed axisymmetric Finite Shell Elements (FSE). In the second, larger part we first will extend the constitutive viscoplastic theory to finite deformation. Then we will present a recently developed shell theory with 7 parameters. We will address the topics of its numerical implementation leading to very efficient FSEs. We

(1) Invited paper presented at the 31st Polish Solid Mechanics Conference in Mierki, Poland.

will present some instructive numerical examples and give an outlook on further research directions in this field.

There exits an almost unlimited literature on elastic shells. For reference purposes, let us cite the papers by NAGHDI [1], VALID [2] and BERNADOU [3]. There also exists a comprehensive literature on rate-independent elastoplastic shells which we will not address here. However, relatively few publications deal with viscoplastic shells. CORMEAU [4] investigates thick elastoplastic shells using a von Mises-type viscoplastic flow rule. He uses general linear shell kinematics and formulates an isoparametric shell element. HUGHES and LIU [5, 6] develop a geometrically nonlinear degenerate shell element. They use a quite general anisotropic viscoplastic constitutive model and solve an impressive number of examples. PARISCH [7] starts as Hughes and Liu from three-dimensional nonlinear continuum mechanics. To account for the nonlinear distribution of the stress components across the shell thickness, he develops a layered model with piecewise linear distributions through the shell thickness. Effectively, his formulation comes close to a fully three-dimensional Finite Element Method (FEM).

KOLLMANN and MUKHERJEE [8] have developed a very general geometrically linear viscoplastic shell theory. They give their entire formulation in rate form and start from a two-field variational principle [9] which for the purely elastic case has been published by ODEN and REDDY [10]. Their shell theory has been used for the formulation of an axisymmetric hybrid strain element by KOLLMANN and BERGMANN [11]. Using the same shell theory, a family of mixed axisymmetric shell elements has been formulated by KOLLMANN *et al.* [12]. KLEIBER and KOLLMANN [13] have extended the shell theory to damage, proposing a generalization of the damage model by GURSON [14]. An and KOLLMANN [15] have suggested a theory of finitely deformed viscoplastic shells.

Finally we will address the formulation of viscoplastic constitutive models. Here we will consider only the so-called *unified models* with internal variables. In such models it is assumed that in the material, inelastic strain rates evolve at any stress level. However, for small stresses these inelastic strain rates are so small that no macroscopically visible inelastic strain is accumulated. Considering this feature, most of such unified models are formulated typically without the notion of a yield surface. Almost all known viscoplastic models are formulated in the context of small strains. Therefore, the total strain rate tensor is decomposed additively into an elastic and an inelastic part. The mathematical model comprises evolution equations for the inelastic strain rates. As arguments of the constitutive functions, not only the stresses appear but also a set of suitably defined internal variables. It is clear that in addition to the evolution of the inelastic strain rates, also evolution equations for these internal variables have to be specified.

A very early model is due to PERZYNA [16]. Further models have been formulated by BODNER and PARTOM [17], CHABOCHE [18], KREMPL and coworkers [19] and STECK [20]. Only very few attempts have been made to generalize viscoplastic constitutive models to finite deformation. RUBIN [21] has extended the model by

Bodner and Partom to finite strains. Following NAGHDI and TRAPP [22], he uses a formulation in strain space. His primary variables are the right Cauchy–Green deformation tensor and its plastic part. Therefore, Rubin gives a formulation on the reference configuration. A formulation on the current configuration has been proposed by NISHIGUCHI *et al.* [23]. They assume *a priori* an additive decomposition of Almansi's strain tensor into an elastic and an inelastic part. The elastic part of the deformation is governed by a hypoplastic constitutive equation. The inelastic constitutive equations are formulated with an unusual objective rate which is an extension of the Jaumann rate. A finite element implementation and numerical examples are presented in [24].

An important issue in finite inelasticity is the time integration of the inelastic constitutive model. Specific considerations have to be taken to fulfill the constraint of inelastic incompressibility. ETEROVIC and BATHE [25] and WEBER and ANAND [26] use the exponential map for this purpose. Further, ETEROVIC and BATHE [25] and MIEHE and STEIN [27] use a logarithmic strain measure. SIMO [28] has systematically exploited the geometric structure of the elastoplastic problem and thus derived compact and closed forms of the tangent operator in the continuous and discrete cases.

2. Theory and numerical analysis of geometrically linear viscoplastic shells

In this section we first describe the essential features of the general inelastic shell theory by KOLLMANN and MUKHERJEE [8]. Then we show the implementation of a family of mixed axisymmetric shell elements. Next, we present the inelastic constitutive model by BODNER and PARTOM [17]. Finally, we give some numerical results.

2.1. Geometrically linear inelastic shell theory

In this section we give a very brief description of the underlying inelastic shell theory [8]. A shell $\mathcal{B}$ is the Cartesian product of a two-dimensional surface $\mathcal{S} \subset \mathbb{R}^3$ with a closed interval $[-h/2, h/2] \subset \mathbb{R}$, i.e.

$$\mathcal{B} := \mathcal{S} \times [-h/2, h/2] \subset \mathbb{R}^3. \tag{2.1}$$

The two-dimensional surface $\mathcal{S}$ is denoted as the shell midsurface (SMS). The quantity h is called the shell thickness. Since in this section a geometrically linear theory is considered, there is no distinction between the actual configuration $\mathcal{B}_t$, $t \in \mathbb{R}$ and the reference configuration $\mathcal{B}_0$ ($\mathcal{B}_0 = \mathcal{B}_t = \mathcal{B}$). We introduce curvilinear coordinates θ^α on $\mathcal{S}$, where Greek indices range from 1 to 2 and Latin ones from 1 to 3. For simplicity it is assumed that the shell thickness is constant on $\mathcal{S}$.

On the SMS covariant and contravariant base vectors $\boldsymbol{A}_\alpha$ and $\boldsymbol{A}^\alpha$ are introduced in a standard manner. The first and second fundamental tensor on the

SMS are denoted by **A** and **B**, respectively. The determinant of the tensor **B** is denoted as B. Next, the normal unit vector A_3 on $\mathcal{S}$ and a normal coordinate z are introduced. The covariant base vectors of the shell space $\mathcal{B}$ are given as

$$G_\alpha = \mathbf{M} A_\alpha , \tag{2.2}$$

$$G_3 = A_3 , \tag{2.3}$$

where

$$\mathbf{M} := \mathbf{I} - z\mathbf{B} \tag{2.4}$$

is the shifter tensor and **I** denotes the unit tensor on $\mathcal{S}$. The determinant of the shifter tensor is given by

$$M = 1 - z\,\mathrm{tr}\,\mathbf{B} + z^2 B, \tag{2.5}$$

where tr denotes the trace operator.

The displacement vector $\boldsymbol{u}^*$ (quantities with a star (as e.g. $\boldsymbol{u}^*$) are referred to the shell space $\mathcal{B}$ while all unstarred quantities (as e.g. $\boldsymbol{u}$) are defined on the SMS $\mathcal{B}$) of any point in the shell space has a representation

$$\boldsymbol{u}^* = \boldsymbol{u} + z\,\boldsymbol{w} , \tag{2.6}$$

where $\boldsymbol{u}$ is the displacement vector of $\mathcal{S}$ and $\boldsymbol{w}$ is the difference vector. In the present paper it is presupposed that the difference vector $\boldsymbol{w}$ is independent of the displacement vector $\boldsymbol{u}$ of the SMS.

The following component representations for the strain tensor $\boldsymbol{\varepsilon}$ in the shell space $\mathcal{B}$ are available [8]

$$\begin{aligned} M\,\varepsilon_{\alpha\beta} &= e_{\alpha\beta} + z\,\kappa_{\alpha\beta} , \\ M\,\varepsilon_{\alpha 3} &= \psi_\alpha + z\,\varrho_\alpha , \\ \varepsilon_{33} &= e_{33} . \end{aligned} \tag{2.7}$$

The quantities $e_{\alpha\beta}$, $\kappa_{\alpha\beta}$, ψ_α and ϱ_α are components of tensor and vector fields, respectively, which are defined on $\mathcal{S}$. Note that the kinematic assumption (2.6) leads to transverse shear strains, which are linear in the normal coordinate z, and to a transverse normal strain which is constant over the shell thickness. We mention that completely analogous relations exist between the velocity field and the strain rate field.

Next a general frame of the inelastic constitutive equations with internal variables is presented. Only such materials are considered which are isotropic and homogeneous. A fundamental constitutive assumption presupposes that the total strain rate tensor $\dot{\boldsymbol{\varepsilon}}$ can be decomposed additively into an elastic and inelastic part

$$\dot{\boldsymbol{\varepsilon}} = \dot{\boldsymbol{\varepsilon}}^{\mathrm{e}} + \dot{\boldsymbol{\varepsilon}}^{\mathrm{n}} . \tag{2.8}$$

The tensor $\dot{\boldsymbol{\varepsilon}}^{\mathrm{e}}$ of the elastic strains is related to the stress rate tensor $\dot{\boldsymbol{\sigma}}$ by Hooke's generalized law

$$\dot{\boldsymbol{\sigma}} = 2G\,\dot{\boldsymbol{\varepsilon}}^{\mathrm{e}} + \lambda(\operatorname{tr}\dot{\boldsymbol{\varepsilon}}^{\mathrm{e}})\,\mathbf{I}\,. \tag{2.9}$$

Here G and λ are the Lamé constants. The inelastic strain rate tensor $\dot{\boldsymbol{\varepsilon}}^{\mathrm{n}}$ obeys in the isothermal case an evolution equation of the following form

$$\dot{\boldsymbol{\varepsilon}}^{\mathrm{n}} = f(\boldsymbol{\sigma}, \boldsymbol{q}^{(k)}), \qquad k = 1, 2, \ldots n\,. \tag{2.10}$$

Here f is a tensor-valued function of the current values of the stress tensor $\boldsymbol{\sigma}$ and a set $\boldsymbol{q}^{(k)}$, $k = 1, 2, \ldots n$ of suitably selected internal variables. The internal variables are either scalars or second order tensors. For these otherwise unspecified internal variables also evolution equations exist

$$\dot{\boldsymbol{q}}^{(k)} = g^{(k)}(\boldsymbol{\sigma}, \boldsymbol{q}^{(r)}), \qquad k, r = 1, 2, \ldots n\,. \tag{2.11}$$

Here again $\boldsymbol{g}^{(k)}$, $k = 1, 2, \ldots n$ denote functions which are depending on the corresponding internal variable $q^{(k)}$ either scalar-valued or tensor-valued.

We introduce vectors (in the sense of matrix calculus) of generalized strain rates $\dot{\boldsymbol{\gamma}}$ and of generalized velocities $\dot{\boldsymbol{v}}$. The relation between the strain rates and the velocities is

$$\dot{\boldsymbol{\gamma}} = \mathbf{L}_{\gamma v}\dot{\boldsymbol{v}}\,, \tag{2.12}$$

where $\mathbf{L}_{\gamma v}$ is a generalized strain-rate velocity operator. The general representation of this operator can be found in [8].

KOLLMANN and MUKHERJEE start from a three-dimensional variational two-field principle [9] which is formulated in velocities and strain rates. Performing the integration over the shell thickness, this variational principle can be reduced to a two-dimensional form. The concise version of the variational principle reads [11]

$$\delta\left\{\int_{\mathcal{S}}\left[\frac{1}{2}\dot{\boldsymbol{\gamma}}^{T}\mathbf{D}_{\gamma\gamma}\,\dot{\boldsymbol{\gamma}} - \dot{\boldsymbol{\gamma}}^{T}\mathbf{D}_{\gamma\gamma}\,\mathbf{L}_{\gamma v}\,\dot{\boldsymbol{v}} + \dot{F}_{L}^{\ T}\dot{\boldsymbol{v}} + \dot{f}^{N^{T}}\mathbf{L}_{\gamma v N}\,\dot{\boldsymbol{v}}\right] dS\right\} = 0. \tag{2.13}$$

Here dS is the area element on the SMS $\mathcal{S}$. Further, $\mathbf{D}_{\gamma\gamma}$ is a generalized elasticity matrix for the shell, $\dot{F}_{L}^{\ T}$ a generalized load rate vector, $\dot{f}^{N^{T}}$ a generalized vector of inelastic pseudo-force rates and $\mathbf{L}_{\gamma v N}$ a linear operator. Details of these objects can be found in [8, 11, 12]. We mention that $\dot{\boldsymbol{\gamma}}$ is the assumed strain rate field while $\dot{\boldsymbol{v}}$ is the velocity field. The assumed strain rate field can be discontinuous between inter-element boundaries.

One principal advantage of the variational principle (2.13) is that it contains only strain rates and velocities but not stress rates. In inelastic shell analysis assumptions such as e.g. (2.6) concerning shell kinematics are generally made. These assumptions lead to information on the distribution of the total strain rates over the shell thickness such as e.g. (2.7). However, unlike the analysis of elastic shells, the distribution of the stresses over the shell thickness is not known *a priori* but it changes in time and space. Therefore, this distribution is a part of the unknown solution. It is not possible to conclude from the stress resultants and moments, which typically evolve from any shell theory including stresses, on the stresses in inelastic shell analysis. It has to be mentioned that KOLLMANN *et al.* [12] have shown in numerical experiments that for elastic shells, stress-like quantities such as e.g. mebrane forces and bending moments exhibit the same order of convergence (with mesh refinements) as the radial deflection of the SMS.

2.2. Implementation of mixed finite shell elements

We start with the discretization of the variational principle (2.13). KOLLMANN and BERGMANN [29] have introduced different shape functions for the generalized velocity vector $\dot{v}$ and the generalized strain rate vector $\dot{\gamma}$

$$\dot{v} = \mathbf{N}\hat{\dot{v}}, \qquad \dot{\gamma} = \overline{\mathbf{N}}\hat{\dot{\gamma}}, \tag{2.14}$$

where a hat ($\hat{}$) indicates nodal values.

Then, the mixed FE model can be derived from the variational principle (2.13) by standard procedures

$$\mathbf{K}_{\gamma\gamma}\hat{\dot{\gamma}} + \mathbf{K}_{\gamma v}\hat{\dot{v}} = \mathbf{0}, \qquad \mathbf{K}_{\gamma v}^{T}\hat{\dot{\gamma}} = -\dot{F}_{\mathrm{L}} - \dot{F}_{\mathrm{N}}, \tag{2.15}$$

where the following quantities have been defined:

$$\begin{aligned}
\mathbf{K}_{\gamma\gamma} &:= \int_{S} \overline{\mathbf{N}}^{\mathrm{T}}\mathbf{D}_{\gamma\gamma}\overline{\mathbf{N}}\,dS,\\
\mathbf{K}_{\gamma v} &:= \int_{S} \overline{\mathbf{N}}^{\mathrm{T}}\mathbf{D}_{\gamma\gamma}\mathbf{L}_{\gamma v}\mathbf{N}\,dS,\\
\dot{F}_{\mathrm{L}} &:= \int_{S} N^{\mathrm{T}}\dot{f}_{\mathrm{L}}\,dS,\\
\dot{F}_{\mathrm{N}} &:= \int_{S} \left(\mathbf{L}_{\gamma v}^{\mathrm{N}}\mathbf{N}\right)^{\mathrm{T}}\dot{f}_{\mathrm{N}}\,dS.
\end{aligned} \tag{2.16}$$

It is possible to find an implementational scheme of the mixed model which fits any FE-code based on the standard displacement formulation. Details of this implementation can be found in [12].

In the following we describe the results obtained for a conical element as originally proposed in the context of the displacement method by ZIENKIEWICZ and coworkers [30] and extended to a mixed hybrid strain formulation by KOLLMANN and BERGMANN [11]. It is important to choose approximations where the polynomial order of the approximation of the strain rate field is at least equal or higher than the approximation of the velocity field. We denote our elements by two numbers, which are separated by the capitals PSS, where PSS indicates that the shell theory is based on the assumption of plane stress and plane strain. The first number indicates the polynomial degree of the shape functions for the strain rate field, and the second one – that of the velocity field. Pursuing numerical tests for elastic cylindrical shells it could be shown that the mixed elements (1PSS1 and 2PSS2) are completely locking free down to a thickness ratio $h/R = 4 \cdot 10^{-10}$, where R is the radius of the cylinder.

2.3. Model of Bodner and Partom for infinitesimal strains

BODNER and PARTOM [17] assume an additive decomposition of the total rate of deformation tensor $\mathbf{d} = \dot{\boldsymbol{\varepsilon}}$ into an elastic and a plastic part

$$\dot{\boldsymbol{\varepsilon}} = \dot{\boldsymbol{\varepsilon}}^{\mathrm{e}} + \dot{\boldsymbol{\varepsilon}}^{\mathrm{p}} . \tag{2.17}$$

We denote the deviator of the stress tensor by $\mathrm{dev}\boldsymbol{\sigma}$. The flow rule takes the form

$$\dot{\boldsymbol{\varepsilon}}^{\mathrm{p}} = \omega \, \mathrm{dev}\boldsymbol{\sigma} . \tag{2.18}$$

HACKENBERG [31] has given the following formulation of this model which is convenient for numerical purposes. Define the following quantities:

$$\begin{aligned} \Pi &:= \sqrt{\frac{3}{2} \mathrm{dev}\boldsymbol{\sigma} : \mathrm{dev}\boldsymbol{\sigma}} = \sqrt{3 J_2} , \\ \dot{\phi} &:= \frac{2}{\sqrt{3}} \sqrt{J_2} \, \omega = \frac{2}{3} \Pi \, \omega , \\ \boldsymbol{\nu} &:= \frac{3}{2} \frac{\mathrm{dev}\boldsymbol{\sigma}}{\Pi} . \end{aligned} \tag{2.19}$$

Then (2.18) can be written as

$$\dot{\boldsymbol{\varepsilon}}^{\mathrm{p}} = \dot{\phi} \boldsymbol{\nu} . \tag{2.20}$$

REMARK 1. Note that (2.20) is the standard form for associative plasticity which is important for time integration. □

REMARK 2. We point out that in our formulation the flow function $\dot{\phi}$ is equal to the equivalent inelastic strain rate. □

The parameter ω in (2.19) is given as

$$\omega = \frac{\sqrt{3}}{\Pi} D_0 \exp\left[-\frac{1}{2}\frac{n+1}{n}\left(\frac{Z}{\Pi}\right)^{2n}\right]. \tag{2.21}$$

The function $\dot{\phi}$ takes the form

$$\dot{\phi} = \frac{2}{\sqrt{3}} D_0 \exp\left[-\frac{1}{2}\frac{n+1}{n}\left(\frac{Z}{\Pi}\right)^{2n}\right]. \tag{2.22}$$

Here Z is an internal variable which models isotropic hardening. The following evolution equation holds for this internal variable

$$\dot{Z} = \frac{m}{Z_0}(Z_1 - Z)\Pi\dot{\phi} \tag{2.23}$$

with initial condition

$$Z\big|_{t=t_0} = Z_0 . \tag{2.24}$$

The quantities D_0, n, m, Z_0 and Z_1 are material parameters which have to be determined from experiments for any material. We note that these parameters are temperature-dependent.

For our numerical work we use parameters given by BODNER and PARTOM [17] for a titanium alloy at room temperature. They are summarized in Table 1. For time integration an implicit algorithm has to be applied as shown e.g. in [32].

Table 1. Material parameters for titanium alloy.

Parameter	Value	Dimension
E	118000	MPa
ν	0.34	–
Z_0	1150	MPa
Z_1	1400	MPa
D_0^2	$1 \cdot 10^8$	s^{-2}
n	1	–
m	100	–

2.4. Numerical results of inelastic computation

As a test example we have computed a cylindrical shell made of the titanium alloy. The shell has an axial length of 1 000 mm, a radius of 250 mm and a thickness of 10 mm. It is closed at its ends. The shell has been discretized using 70 equally spaced 1PSS1 elements. The loading history of the shell is depicted in Fig. 1. The

internal pressure is increased within 1 s linearly from zero to the maximal value of 13.0 MPa. Then this pressure is held constant over the time of 9 s. Finally, the pressure drops linearly within 1 s to zero. In Fig. 2 the deflection of the shell is depicted for the following times: $t = 0.55$ s, $t = 5$ s, $t = 5.55$ s and $t = 10$ s.

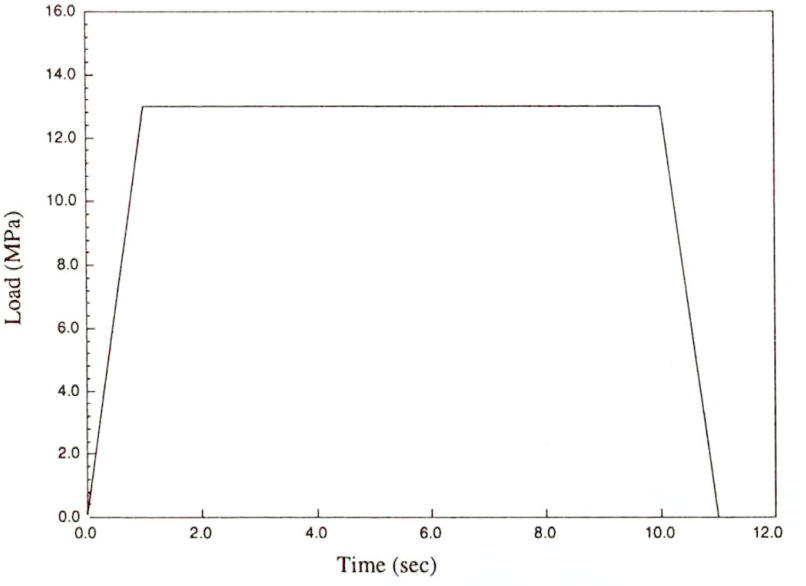

FIG. 1. Load-history for the cylindrical shell.

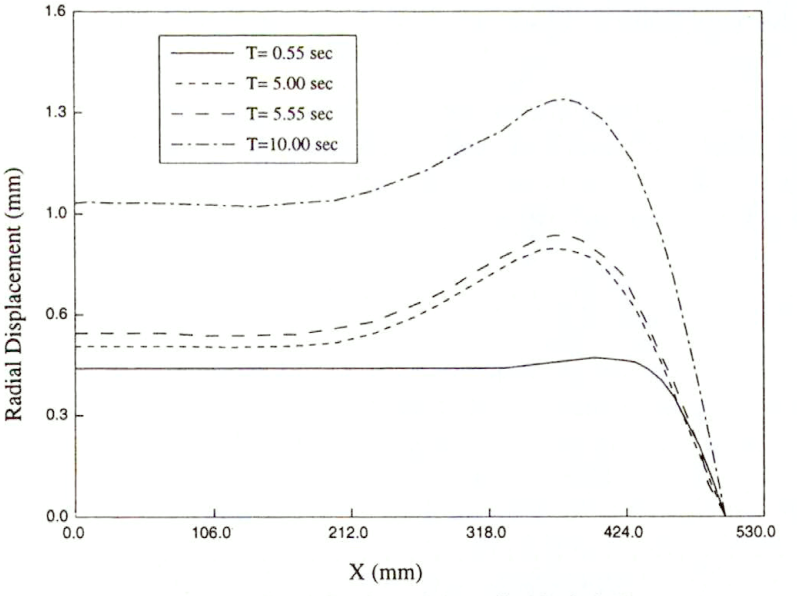

FIG. 2. Radial deflection of the cylindrical shell.

At $t = 1\,\mathrm{s}$ the loading of the shell is completed. In the middle section a pure membrane deformation prevails. Only at the edge in the region $350\,\mathrm{mm} \leq z \leq 400\,\mathrm{mm}$ bending effects can be noticed. During the hold time $1\,\mathrm{s} \leq t \leq 100\,\mathrm{s}$ considerable additional deformation due to viscoplastic effects takes place. It is remarkable that the region of noticeable bending effects spreads into the interior of the shell. During unloading ($10\,\mathrm{s} \leq t \leq 11\,\mathrm{s}$) the elastic part of the deformation is recovered. After unloading no additional inelastic deformation can be observed.

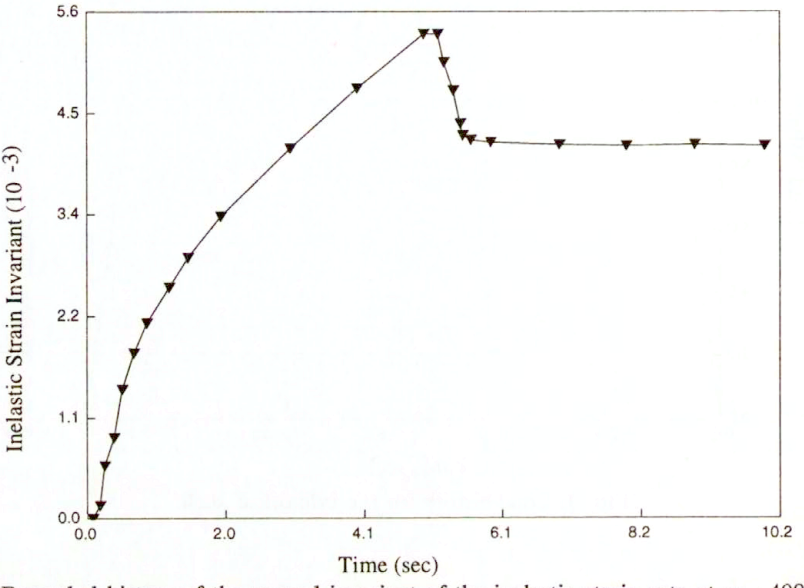

FIG. 3. Recorded history of the second invariant of the inelastic strain rate at $z = 408.948\,\mathrm{mm}$ and $r = 254.840\,\mathrm{mm}$.

Figure 3 shows the recorded history of the development of the second invariant of the inelastic strain rate tensor at a point of the shell ($z = 408.943\,\mathrm{mm}$, $r = 254.840\,\mathrm{mm}$), where bending effects dominate. The second invariant of the inelastic strain rate is defined as

$$I_2(\dot{\boldsymbol{\varepsilon}}^{\mathrm{p}}) := \sqrt{\frac{2}{3}\dot{\boldsymbol{\varepsilon}}^{\mathrm{p}} : \dot{\boldsymbol{\varepsilon}}^{\mathrm{p}}}\,. \tag{2.25}$$

During the first second of the loading history the equivalent inelastic strain rate is very small. Then it increases sharply with time. At the beginning of the hold time the second invariant of the inelastic strain rate drops continuously. With unloading it sharply drops to zero.

Finally in Fig. 4 the distribution of the axial bending stress σ_{zz} over the thickness of the shell at $z = 408.943\,\mathrm{mm}$ is given.

At $t = 0.55\,\mathrm{s}$ during the loading period the distribution of the stress is linear, i.e. the deformation is purely elastic. At the end of the loading phase $t = 1.0\,\mathrm{s}$,

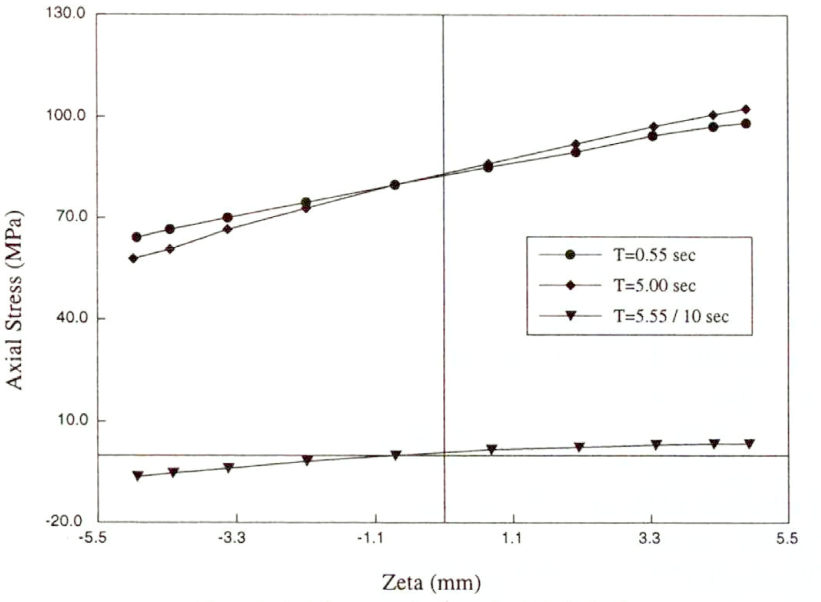

FIG. 4. Axial stress of the cylindrical shell.

a slight curvature of the stress distribution can be observed. During the hold time until $t = 10\,\mathrm{s}$, a redistribution of the bending stress occurs and the curvature of the stress distribution is increased. Finally after unloading at $t = 11\,\mathrm{s}$ the residual stress has developed. It has to be noticed that in the theory of Bodner and Partom, neither loading or unloading conditions nor a yield surface are present.

3. Finite deformation of three-dimensional viscoplastic continua

In this section we present a concise theory of a finitely deformed elasto-viscoplastic continuum. Then we apply this theory for an extension of the infinitesimal viscoplastic model by Bodner and Partom to finite deformation.

3.1. Three-dimensional elasto-viscoplastic continuum under finite deformation

After consideration of finite deformation of viscoplastic bodies we discuss in general the elastic and viscoplastic constitutive models. Then a hyperelastic model and a generalization of the model of Bodner and Partom presented in Sec. 2.3 will be given.

3.1.1. Kinematics of finitely deformed elasto-viscoplastic bodies. A motion of the body B is a one parameter mapping $\phi_t : \mathcal{B}_0 \to \mathcal{B}_t$ where $t \in \mathbb{R}$ is the time and $\mathcal{B}_t$ is the current configuration at time t. For any $X \in \mathcal{B}_0$ we have $\phi(X) = \boldsymbol{x} \in \mathcal{B}_t$. For any $X \in B$ we denote the tangent spaces of the reference and current configuration

as $T_X\mathcal{B}_0$ and $T_x\mathcal{B}_t$, respectively, and the coordinate charts, which are taken to be convected, by θ^i. The deformation gradient is defined as

$$\begin{aligned} &\mathbf{F} := T_X\mathcal{B}_0 \to T_x\mathcal{B}_t\,, \\ &\mathbf{F} = T\boldsymbol{\phi} = \boldsymbol{g}_i \otimes \boldsymbol{G}^i, \qquad i = 1,2,3, \end{aligned} \tag{3.1}$$

where we have $\boldsymbol{G}_i = \mathbf{X}_{,i}$, $\boldsymbol{g}_i = \mathbf{x}_{,i}$, $\boldsymbol{G}_i \cdot \boldsymbol{G}^j = \delta_i^j$, $\boldsymbol{g}_i \cdot \boldsymbol{g}^j = \delta_i^j$. Here, derivatives with respect to θ^i are denoted by a comma, scalar product of vectors by a dot, and δ_i^j is the Kronecker delta.

Note that the deformation gradient is a two-point tensor. Further note, that we have suppressed in (3.1) the dependence of the deformation gradient on time.

It is convenient to introduce the right Cauchy–Green deformation tensor as

$$\mathbf{C} = \mathbf{F}^T \mathbf{g}\, \mathbf{F}\,, \tag{3.2}$$

where $\mathbf{g}$ is the metric tensor in the current configuration $\mathcal{B}_t$. Speaking in geometric terms [33], the right-hand side of (3.2) can be interpreted as the pull-back of the metric tensor of the current configuration to the reference configuration, i.e. $\mathbf{C} = \phi^*(\mathbf{g})$.

Next we introduce the multiplicative decomposition [34, 35, 36] of the deformation gradient into an elastic and a plastic part

$$\mathbf{F} = \mathbf{F}_\mathrm{e}\, \mathbf{F}_\mathrm{p}\,, \tag{3.3}$$

where the assumed incompressibility of the inelastic deformations means that $\mathbf{F}_\mathrm{p} \in SL^+(3,\mathbb{R})$, $SL^+(3,\mathbb{R})$ denotes the special linear group with determinant equal one.

REMARK 3. The multiplicative decomposition (3.3) is often accepted as equivalent with the introduction of an intermediate configuration $\widehat{\mathcal{B}}$. In contrast to this understanding which has caused a lot of discussion in the literature, we define

$$\begin{aligned} &\mathbf{F}_\mathrm{p} := T_X\mathcal{B}_0 \to T_X\mathcal{B}_0\,, \\ &\mathbf{F}_\mathrm{e} := T_X\mathcal{B}_0 \to T_x\mathcal{B}_t\,. \end{aligned} \tag{3.4}$$

That is, the inelastic part of the deformation gradient is a map from $T_X\mathcal{B}_0$ onto itself. It is, accordingly, a material tensor uniquely defined by the evolution equation of an appropriately defined material plastic rate. If the constraint of plastic incompressibility is assumed, then $\det \mathbf{F}_\mathrm{p} = 1$ holds; i.e. $\mathbf{F}_\mathrm{p}$ is an unimodular tensor. □

Equation (3.3) motivates the introduction of an elastic and a plastic right Cauchy–Green deformation tensor

$$\begin{aligned} \mathbf{C}_\mathrm{e} &:= \mathbf{F}_\mathrm{e}^\mathrm{T} \mathbf{g}\, \mathbf{F}_\mathrm{e}\,, \\ \mathbf{C}_\mathrm{p} &:= \mathbf{F}_\mathrm{p}^\mathrm{T} \mathbf{F}_\mathrm{p}\,. \end{aligned} \tag{3.5}$$

The elastic right Cauchy–Green deformation tensor $\mathbf{C}_e$ can be interpreted as pull-back of the metric tensor $\mathbf{g}$ with the elastic part $\mathbf{F}_e$ of the deformation gradient.

The deformation gradient $\mathbf{F}$ is an element of the general linear group $GL^+(3,\mathbb{R})$ with positive determinant. Therefore, we can attribute to its time derivative a left and right rate

$$\begin{aligned} \dot{\mathbf{F}} &= \mathbf{l}\mathbf{F}, \\ \dot{\mathbf{F}} &= \mathbf{F}\mathbf{L}. \end{aligned} \tag{3.6}$$

Both rates are mixed tensors (contravariant-covariant). They are related by means of the equation

$$\mathbf{L} = \mathbf{F}^{-1}\mathbf{l}\mathbf{F}. \tag{3.7}$$

Geometrically Eq. (3.7) is the pull-back of the mixed velocity gradient from the current configuration to the reference configuration, i.e. $\mathbf{L} = \phi^*(\mathbf{l})$.

Since $\mathbf{F}_p \in SL^+(3,\mathbb{R})$, we can again define a right rate according to

$$\dot{\mathbf{F}}_p = \mathbf{F}_p \mathbf{L}_p \tag{3.8}$$

which proves to be more appropriate for a numerical treatment in a purely material context. If a constitutive function is specified for the right rate $\mathbf{L}_p$ of the plastic part $\mathbf{F}_p$ of the deformation gradient, then Eq. (3.8) constitutes an evolution equation for $\mathbf{F}_p$.

3.2. Elasto-viscoplastic constitutive model

We start with general considerations where we use thermodynamical arguments to formulate a general frame for the elastic part of the constitutive model. Then we modify the elastic model for the sake of numerical efficiency. Next, the infinitesimal model of Bodner and Partom presented in Sec. 2.3 is modified and generalized to finite strains.

3.2.1. General considerations. Let $\boldsymbol{\tau}$ be the Kirchhoff stress tensor. Consider the expression of the internal power

$$\mathcal{W} = \boldsymbol{\tau} : \mathbf{l}, \tag{3.9}$$

where $\mathbf{l}$ is defined in $(3.6)_1$ and the relation holds: $\mathbf{a} : \mathbf{b} = \operatorname{tr} \mathbf{a}\mathbf{b}^t$ for $\mathbf{a}$, $\mathbf{b}$ being second order tensors and tr denoting the trace operation. The expression is rewritten using material tensors as

$$\mathcal{W} = \boldsymbol{\Xi} : \mathbf{L}. \tag{3.10}$$

The comparison of (3.9) with (3.10) leads with the aid of (3.7) to the definition of the material stress tensor

$$\Xi = \phi^*(\tau) = \mathbf{F}_p^T \tau \mathbf{F}_p^{-T}. \tag{3.11}$$

The tensor Ξ is, accordingly, the mixed variant pull-back of the Kirchhoff tensor. It coincides with Noll's intrinsic stress tensor and some authors call it Mandel's stress tensor.

A common feature of unified inelastic constitutive models is the introduction of phenomenological internal variables. We denote a typical internal variable by $\mathbf{Z}$. Assuming the existence of a free energy function according to $\psi = \psi(\mathbf{C}_e, \mathbf{Z})$, the localised form of the dissipation inequality for an isothermal process takes the form

$$\begin{aligned} \mathcal{D} &= \tau : \mathbf{l} - \varrho_{ref} \dot{\psi} \\ &= \Xi : \mathbf{L} - \varrho_{ref} \dot{\psi} \geq 0, \end{aligned} \tag{3.12}$$

where ϱ_{ref} is the density at the reference configuration.

Making use of the relation

$$\dot{\mathbf{C}}_e = \mathbf{F}_p^{-T} \mathbf{L}^T \mathbf{C} \mathbf{F}_p^{-1} + \mathbf{F}_p^{-T} \mathbf{C} \mathbf{L} \mathbf{F}_p^{-1} - \mathbf{F}_p^{-T} \mathbf{L}_p^T \mathbf{C} \mathbf{F}_p^{-1} - \mathbf{F}_p^{-T} \mathbf{C} \mathbf{L}_p \mathbf{F}_p^{-1} \tag{3.13}$$

one may derive

$$\dot{\psi} = 2\mathbf{C} \mathbf{F}_p^{-1} \frac{\partial \psi}{\partial \mathbf{C}_e} \mathbf{F}_p^{-T} : (\mathbf{L} - \mathbf{L}_p) + \frac{\partial \psi}{\partial \mathbf{Z}} \cdot \dot{\mathbf{Z}}. \tag{3.14}$$

Insertion of (3.14) into (3.12) leads to

$$\begin{aligned} \mathcal{D} = \left(\Xi - 2\varrho_{ref} \mathbf{C} \mathbf{F}_p^{-1} \frac{\partial \psi(\mathbf{C}_e, \mathbf{Z})}{\partial \mathbf{C}_e} \mathbf{F}_p^{-T} \right) : \mathbf{L} \\ + 2\varrho_{ref} \mathbf{C} \mathbf{F}_p^{-1} \frac{\partial \psi(\mathbf{C}_e, \mathbf{Z})}{\partial \mathbf{C}_e} \mathbf{F}_p^{-T} : \mathbf{L}_p - \varrho_{ref} \frac{\partial \psi(\mathbf{C}_e, \mathbf{Z})}{\partial \mathbf{Z}} \cdot \mathbf{Z} \geq 0. \end{aligned} \tag{3.15}$$

By defining Y as the thermodynamical force conjugate to the internal variable $\mathbf{Z}$

$$Y := -\varrho_{ref} \frac{\partial \psi(\mathbf{C}_e, \mathbf{Z})}{\partial \mathbf{Z}}, \tag{3.16}$$

and making use of standard thermodynamical arguments, from (3.15) follows the elastic constitutive equation

$$\Xi = 2\varrho_{ref} \mathbf{C} \mathbf{F}_p^{-1} \frac{\partial \psi(\mathbf{C}_e, \mathbf{Z})}{\partial \mathbf{C}_e} \mathbf{F}_p^{-T} = 2\varrho_{ref} \mathbf{F}_p^T \mathbf{C}_e \frac{\partial \psi(\mathbf{C}_e, \mathbf{Z})}{\partial \mathbf{C}_e} \mathbf{F}_p^{-T} \tag{3.17}$$

as well as the reduced local dissipation inequality

$$\mathcal{D}_{\mathrm{p}} := \boldsymbol{\Xi} : \mathbf{L}_{\mathrm{p}} + \boldsymbol{Y} : \dot{\mathbf{Z}} \geq 0, \tag{3.18}$$

where (3.16) has been considered. $\mathcal{D}_{\mathrm{p}}$ is the plastic dissipation function. From (3.18) follows an essential result that the stress tensor $\boldsymbol{\Xi}$ and the plastic rate $\mathbf{L}_{\mathrm{p}}$ are conjugate variables. Observe that the tensor $\mathbf{L}_{\mathrm{p}}$ is defined in (3.8).

3.2.2. The elastic constitutive model. We assume that the elastic potential can be decomposed additively into one part depending only on the elastic right Cauchy–Green deformation tensor $\mathbf{C}_e$ and the other one depending only on the internal variable $\mathbf{Z}$

$$\psi = \psi_{\mathrm{e}}(\mathbf{C}_e) + \psi_{\mathrm{Z}}(\mathbf{Z}). \tag{3.19}$$

Defining the logarithmic strain measure

$$\boldsymbol{\alpha} := \ln \mathbf{C}_{\mathrm{e}}, \qquad \mathbf{C}_{\mathrm{e}} = \exp \boldsymbol{\alpha} \tag{3.20}$$

and assuming that the material is elastically isotropic, one can prove that the relation holds

$$\mathbf{C}_{\mathrm{e}} \frac{\partial \psi_{\mathrm{e}}(\mathbf{C}_{\mathrm{e}})}{\partial \mathbf{C}_{\mathrm{e}}} = \frac{\partial \psi_{\mathrm{e}}(\boldsymbol{\alpha})}{\partial \boldsymbol{\alpha}}, \tag{3.21}$$

where $\psi_{\mathrm{e}}(\alpha)$ is the potential expressed in the logarithmic strain measure $\boldsymbol{\alpha}$. The proof is given in [37]. Equation (3.17) results then in

$$\boldsymbol{\Xi} = 2\varrho_{\mathrm{ref}} \mathbf{F}_{\mathrm{p}}^{\mathrm{T}} \frac{\partial \psi_{\mathrm{e}}(\boldsymbol{\alpha})}{\partial \boldsymbol{\alpha}} \mathbf{F}_{\mathrm{p}}^{-\mathrm{T}}. \tag{3.22}$$

Note that ψ_{e} is an isotropic function of $\boldsymbol{\alpha}$. The last equation motivates the introduction of a modified logarithmic strain measure

$$\overline{\boldsymbol{\alpha}} := \mathbf{F}_{\mathrm{p}}^{-1} \boldsymbol{\alpha} \mathbf{F}_{\mathrm{p}}. \tag{3.23}$$

Since the following relation for the exponential map holds

$$\mathbf{F}_{\mathrm{p}}^{-1}(\exp \boldsymbol{\alpha}) \mathbf{F}_{\mathrm{p}} = \exp \overline{\boldsymbol{\alpha}}, \tag{3.24}$$

Eq. (3.22) takes the form

$$\boldsymbol{\Xi} = 2\varrho_{\mathrm{ref}} \frac{\partial \psi(\overline{\boldsymbol{\alpha}})}{\partial \overline{\boldsymbol{\alpha}}}. \tag{3.25}$$

REMARK 4. A comparison of (3.17) and (3.25) reveals the computational advantages of the latter formulation. For evaluation of (3.17) the inverse of the

tensor $\mathbf{F}_p^T$ has to be computed. The final expression for (3.25) contains only the derivative of the elastic potential with respect to the modified logarithmic strain tensor $\overline{\boldsymbol{\alpha}}$. □

It is interesting to note that (3.24) together with (3.20), (3.2), and $(3.5)_2$ lead to a direct definition of $\overline{\boldsymbol{\alpha}}$. The relation holds

$$\overline{\boldsymbol{\alpha}} = \ln(\mathbf{C}_p^{-1}\mathbf{C}). \tag{3.26}$$

For computational simplicity a linear relation is assumed and, therefore, the elastic constitutive model (3.25) takes its final form

$$\boldsymbol{\Xi} = K \operatorname{tr}\overline{\boldsymbol{\alpha}}^T \mathbf{1} + \mu \operatorname{dev}\overline{\boldsymbol{\alpha}}^T, \tag{3.27}$$

where

$$\overline{\boldsymbol{\alpha}}^T = \ln(\mathbf{C}\,\mathbf{C}_p^{-1}), \tag{3.28}$$

K is the bulk modulus and μ the shear modulus.

3.2.3. Extended model of Bodner and Partom. We make now use of the form of the inelastic constitutive model of BODNER and PARTOM [17]. In Sec. 3.2.1 we concluded from (3.18) that the tensors $\boldsymbol{\Xi}$ and $\mathbf{L}_p$ are conjugate. A basic issue is now to put the mentioned constitutive model into a frame which is compatible with this fact. Essentially we have to consider the stress tensor $\boldsymbol{\Xi}$ as the driving stress quantity while the plastic rate for which an evolution equation is to be formulated is taken to be $\mathbf{L}_p$. We, therefore, derive the finite formulation of Eqs. (3.19), (3.20) by the substitutions

$$\begin{aligned} \boldsymbol{\sigma} &\to \boldsymbol{\Xi}, \\ \dot{\boldsymbol{\varepsilon}}^p &\to \mathbf{L}_p^T. \end{aligned} \tag{3.29}$$

This leads to the following set of evolution equations

$$\mathbf{L}_p = \dot{\phi}\boldsymbol{\nu}^T; \tag{3.30}$$

$$\begin{aligned} \dot{Z} &= \frac{M}{Z_0}(Z_1 - Z)\dot{W}_p, \\ \dot{W}_p &= \Pi\dot{\phi}(\Pi, Z), \\ \Pi &= \sqrt{\frac{3}{2}\operatorname{dev}\boldsymbol{\Xi} : \operatorname{dev}\boldsymbol{\Xi}}, \\ \dot{\phi} &= \frac{2}{\sqrt{3}} D_0 \exp\left[-\frac{1}{2}\frac{N+1}{N}\left(\frac{Z}{\Pi}\right)^{2N}\right], \\ \boldsymbol{\nu} &= \frac{3}{2}\frac{\operatorname{dev}\boldsymbol{\Xi}}{\Pi}. \end{aligned} \tag{3.31}$$

Here, Z_0, Z_1, D_0, N, M are material parameters.

The choice of the transposed quantity in (3.20) is motivated by the updating formula for the stress tensor which is given in Sec. 4, Eq. (4.31). Moreover, the generalization of a flow rule of the more classical von Mises type to nonsymmetric arguments would lead to a flow rule of the form (3.30). Thus, the flow rule chosen fits the classical models of associated viscoplasticity.

Note that by its very definition in (3.11), the tensor $\boldsymbol{\Xi}$ is physically equivalent to the Kirchhoff stress tensor in the sense that both have the same invariants.

4. The nonlinear shell theory

After presenting basic features of the theory of finitely deformed shells, let us now give some details of a new shell model containing 7 parameters. Then the reduction of the three-dimensional principle of virtual work to a shell formulation will be presented.

4.1. Preliminaries of finite shell theory

We adopt the definition (2.1). However, we distinguish carefully between the reference configuration $\mathcal{B}_0$ and the current configuration $\mathcal{B}_t$. For any $X \in \mathcal{B}$ and any $\boldsymbol{x} \in \mathcal{B}_t$ we recall the relations for the tangent base vectors at the reference and actual configurations

$$G_i = X_{,i}\,, \qquad \boldsymbol{g}_i = \boldsymbol{x}_{,i}. \tag{4.1}$$

The corresponding metrics at the actual and the reference configurations are denoted by $\mathbf{g}$ and $\mathbf{G}$, respectively. Their components are given by $\mathrm{G}_{ij} = \boldsymbol{G}_i \cdot \boldsymbol{G}_j$ and $\mathrm{g}_{ij} = \boldsymbol{g}_i \cdot \boldsymbol{g}_j$, respectively.

As in Sec. 2, we introduce in the reference configuration the shell midsurface as reference surface $\mathcal{M}$ where we again presuppose constant shell thicknes h. Following the standards, the coordinate ϑ^3 perpendicular to $\mathcal{M}$, will now be denoted by $z \in [-h/2, h/2]$, $h \in \mathbb{R}^+$, and the tangent vectors of $\mathcal{TM}$ in the undeformed reference configuration by $\boldsymbol{A}_\alpha$ ($\alpha = 1, 2$) and $\boldsymbol{N}$, with $\boldsymbol{N} \cdot \boldsymbol{A}_\alpha = 0$. We denote their image at an actual configuration by $\boldsymbol{a}_\alpha$ and $\boldsymbol{a}_3$, where in general $\boldsymbol{a}_3 \cdot \boldsymbol{a}_\alpha \neq 0$ and $|\boldsymbol{a}_3| \neq 1$. Thus we have $\boldsymbol{A}_\alpha = \boldsymbol{G}_\alpha|_{z=0}$ and $\boldsymbol{a}_\alpha = \boldsymbol{g}_\alpha|_{z=0}$. Further, $\mathbf{A}$ refers to the metric of the reference midsurface with covariant components $\mathrm{A}_{\alpha\beta} = \boldsymbol{A}_\alpha \cdot \boldsymbol{A}_\beta$, $\mathrm{a}_{\alpha\beta}$ are then the related components at the actual configuration. Their contravariant counterparts are denoted as usual by $\mathrm{A}^{\alpha\beta}$ and $\mathrm{a}^{\alpha\beta}$.

In addition to the curvilinear base vectors, we consider the fixed Cartesian frame $\boldsymbol{e}_i$ and define the quantities

$$\mathrm{c}_{\alpha i} = \boldsymbol{A}_\alpha \cdot \boldsymbol{e}_i\,, \qquad \mathrm{c}_{3i} = \boldsymbol{N} \cdot \boldsymbol{e}_i\,, \tag{4.2}$$

to get the following relations

$$\boldsymbol{A}_\alpha = \mathrm{c}_{\alpha i}\boldsymbol{e}_i\,, \qquad \boldsymbol{N} = \mathrm{c}_{3i}\boldsymbol{e}_i\,, \qquad \text{and} \qquad \boldsymbol{e}_i = \mathrm{c}_{\alpha i}\boldsymbol{A}^\alpha + \mathrm{c}_{3i}\boldsymbol{N}, \tag{4.3}$$

which will be of use later on.

By **B** we denote the two-dimensional curvature tensor of the undeformed reference surface with components $B_{\alpha\beta} = -A_\alpha \cdot N_{,\beta}$. We also make use of the shifter tensor **M** (see Eq. (2.4)) and its determinant M (see Eq. (2.5)). The following exact expressions hold

$$
\begin{aligned}
G_\alpha &= A_\alpha + zN_{,\alpha} = (\mathbf{I} - z\mathbf{B})A_\alpha = \mathbf{M}A_\alpha, \\
G^\alpha &= \mathbf{M}^{-1}A^\alpha, \qquad G_3 = N.
\end{aligned} \tag{4.4}
$$

4.2. Shell strain measures

The shell theory is based on the following fundamental assumption. We assume that any configuration of the shell space is determined by the equation

$$
\boldsymbol{x}(\vartheta^\alpha, z) = \boldsymbol{x}^0(\vartheta^\alpha) + (z + z^2\chi(\vartheta^\alpha))\boldsymbol{a}_3(\vartheta^\alpha), \tag{4.5}
$$

where $\boldsymbol{x}^0$ denotes the corresponding configuration of the midsurface. Then the ordered triple $(\boldsymbol{x}^0, \boldsymbol{a}_3, \chi)$ defines the configuration space of the shell.

The following basic features of the above assumption are pointed out:

1. The assumed shell kinematics belongs to a general class given by the relation $\boldsymbol{x}(\vartheta^\alpha, z) = \boldsymbol{x}^0(\vartheta^\alpha) + f(z)\boldsymbol{a}_3(\vartheta^\alpha)$ where $f(z)$ can be an arbitrary function of z. This class of kinematics differs entirely from that used e.g. by NAGHDI [1], where $\boldsymbol{x}$ is expanded into a series of z.

2. The assumed shell kinematics is the simplest possible which allows for a linear distribution of the transverse strains (shear and normal) over the shell thickness. The constant part of transverse strains over the shell thickness is described by $\mathbf{a}_3$ whereas χ determines the linearly varying part. Note that fibres perpendicular to the reference midsurface $\mathcal{M}$ remain *straight* after the deformation.

3. As a consequence, three-dimensional constitutive equations can be applied. Accordingly, the formulation is suitable for small as well as for large strain cases in elasticity or elasto-viscoplasticity.

4. The shell kinematics enables to circumvent the use of a rotation tensor. Shell formulations using a rotation tensor with 5 parameters as in [38, 39, 40] or with 6 parameters as in [41, 42, 43, 44] does not furnish directly information about the tranversal strains in thickness direction. Such an information is obtained using further constitutive assumptions such as incompressibility or plane stress assumption. Accordingly, formulations with a rotation tensor, besides being complicated due to the structure of the rotation group, seem to be less adequate for the object of this paper. In addition, as previous numerical studies show, in the present formulation the limit case of very thin shells can be achieved without loss of accuracy.

By (4.1) and (4.5) the tangent vectors become

$$
\begin{aligned}
\boldsymbol{g}_\alpha &= \frac{\partial \boldsymbol{x}^0}{\partial \vartheta^\alpha} + (z + z^2\chi)\frac{\partial \boldsymbol{a}_3}{\partial \vartheta^\alpha} + z^2\frac{\partial \chi}{\partial \vartheta^\alpha}\boldsymbol{a}_3 \\
&= \boldsymbol{a}_\alpha + (z + z^2\chi)\boldsymbol{a}_{3,\alpha} + z^2\chi_{,\alpha}\boldsymbol{a}_3\,, \qquad (4.6)\\
\boldsymbol{g}_3 &= (1 + 2z\chi)\boldsymbol{a}_3\,.
\end{aligned}
$$

For the deformation gradient defined in $(3.1)_2$ we obtain

$$
\begin{aligned}
\mathbf{F} &= \boldsymbol{g}_\alpha \otimes \boldsymbol{G}^\alpha + \boldsymbol{g}_3 \otimes \boldsymbol{N} \qquad (4.7)\\
&= \boldsymbol{a}_\alpha \otimes \boldsymbol{G}^\alpha + \left[(z + z^2\chi)\boldsymbol{a}_{3,\alpha} + z^2\chi_{,\alpha}\boldsymbol{a}_3\right] \otimes \boldsymbol{G}^\alpha + (1 + 2z\chi)\boldsymbol{a}_3 \otimes \boldsymbol{N}\,.
\end{aligned}
$$

By defining the tangent map of the midsurface $\mathbf{F}^0 := \mathbf{F}|_{z=0}$

$$
\mathbf{F}^0 := \boldsymbol{a}_\alpha \otimes \boldsymbol{A}^\alpha + \boldsymbol{a}_3 \otimes \boldsymbol{N}\,, \qquad (4.8)
$$

with $\boldsymbol{a}_\alpha = \mathbf{F}^0\boldsymbol{A}_\alpha$, $\boldsymbol{a}_3 = \mathbf{F}^0\boldsymbol{N}$ and by defining further the tensors

$$
\begin{aligned}
\mathbf{b} &= \boldsymbol{a}_{3,\alpha} \otimes \boldsymbol{A}^\alpha + 2\chi\boldsymbol{a}_3 \otimes \boldsymbol{N}, \qquad (4.9)\\
\mathbf{c} &= (\chi\boldsymbol{a}_{3,\alpha} + \chi_{,\alpha}\boldsymbol{a}_3) \otimes \boldsymbol{A}^\alpha,
\end{aligned}
$$

we arrive at the following expression for $\mathbf{F}$:

$$
\mathbf{F} = (\mathbf{F}^0 + z\mathbf{b} + z^2\mathbf{c})\mathbf{M}^{-1}. \qquad (4.10)
$$

Next, we introduce the displacement field $\boldsymbol{u}^0$ for the SMS and the difference vector $\boldsymbol{w}$ as

$$
\begin{aligned}
\boldsymbol{u}^0 &:= \boldsymbol{x}^0 - \boldsymbol{X}^0, \qquad (4.11)\\
\boldsymbol{w} &:= \boldsymbol{a}_3 - \boldsymbol{N}\,,
\end{aligned}
$$

with $\boldsymbol{X}^0$ being a point on the reference surface $\mathcal{M}$. With (4.11), it follows from (4.8) and (4.9) that

$$
\begin{aligned}
\mathbf{F}^0 &= (\boldsymbol{A}_\alpha + \boldsymbol{u}^0_{,\alpha}) \otimes \boldsymbol{A}^\alpha + (\boldsymbol{N} + \boldsymbol{w}) \otimes \boldsymbol{N}\,, \qquad (4.12)\\
\mathbf{b} &= -\mathbf{B} + \boldsymbol{w}_{,\alpha} \otimes \boldsymbol{A}^\alpha + 2\chi(\boldsymbol{N} + \boldsymbol{w}) \otimes \boldsymbol{N}\,,\\
\mathbf{c} &= -\chi\mathbf{B} + [\chi\boldsymbol{w}_{,\alpha} + \chi_{,\alpha}(\boldsymbol{N} + \boldsymbol{w})] \otimes \boldsymbol{A}^\alpha.
\end{aligned}
$$

Making use of (4.10), the right Cauchy–Green strain tensor of the shell space given in (3.2) takes the form

$$
\begin{aligned}
\mathbf{C} = \mathbf{M}^{-\mathrm{T}}\big[&\mathbf{F}^{0\mathrm{T}}\mathbf{F}^0 + z(\mathbf{F}^{0\mathrm{T}}\mathbf{b} + \mathbf{b}^{\mathrm{T}}\mathbf{F}^0) + z^2(\mathbf{b}^{\mathrm{T}}\mathbf{b} + \mathbf{F}^{0\mathrm{T}}\mathbf{c} + \mathbf{c}^{\mathrm{T}}\mathbf{F}^0) \qquad (4.13)\\
&+ z^3(\mathbf{b}^{\mathrm{T}}\mathbf{c} + \mathbf{c}^{\mathrm{T}}\mathbf{b}) + z^4\mathbf{c}^{\mathrm{T}}\mathbf{c}\big]\,\mathbf{M}^{-1}.
\end{aligned}
$$

The last expression motivates the definitions

$$\begin{aligned} \mathbf{C}^0 &:= \mathbf{F}^{0\mathrm{T}}\mathbf{F}^0, \\ \mathbf{K} &:= \mathbf{F}^{0\mathrm{T}}\mathbf{b} + \mathbf{b}^{\mathrm{T}}\mathbf{F}^0 \end{aligned} \tag{4.14}$$

with the help of which we write for (4.13)

$$\mathbf{C} = \mathbf{M}^{-\mathrm{T}}\left[\mathbf{C}^0 + z\mathbf{K} + \ldots\right]\mathbf{M}^{-1}. \tag{4.15}$$

In what follows we assume that the shell is thin in the sense that only the first two strain measures $\mathbf{C}^0$ and $\mathbf{K}$ are dominant. The inclusion of all other strain measures is of course possible but is left out for the sake of simplicity.

We consider now the following decompositions

$$\boldsymbol{u}^0 = u_i \boldsymbol{e}_i\,, \qquad \boldsymbol{w} = w_i \boldsymbol{e}_i\,. \tag{4.16}$$

Then the tensors $\mathbf{C}^0$ $(4.14)_1$ and $\mathbf{K}$ $(4.14)_2$ take the form

$$\begin{aligned} \mathbf{C}^0 &= \mathrm{C}_{\alpha\beta}\boldsymbol{A}^\beta \otimes \boldsymbol{A}^\alpha + \mathrm{C}_{3\alpha}\boldsymbol{A}^\alpha \otimes \boldsymbol{N} + \mathrm{C}_{\alpha 3}\boldsymbol{N} \otimes \boldsymbol{A}^\alpha + \mathrm{C}_{33}\boldsymbol{N} \otimes \boldsymbol{N}, \\ \mathbf{K} &:= \mathrm{K}_{\alpha\beta}\boldsymbol{A}^\beta \otimes \boldsymbol{A}^\alpha + \mathrm{K}_{3\alpha}\boldsymbol{A}^\alpha \otimes \boldsymbol{N} + \mathrm{K}_{\alpha 3}\boldsymbol{N} \otimes \boldsymbol{A}^\alpha + \mathrm{K}_{33}\boldsymbol{N} \otimes \boldsymbol{N}. \end{aligned} \tag{4.17}$$

Considering (4.16), the following representations of the components in (4.17) based on the Cartesian components (4.16) can be obtained [45]:

$$\begin{aligned} \mathrm{C}_{\alpha\beta} &= \mathrm{A}_{\alpha\beta} + \mathrm{c}_{\beta i}u_{i,\alpha} + \mathrm{c}_{\alpha i}u_{i,\beta} + u_{i,\alpha}u_{i,\beta}\,, \\ \mathrm{C}_{\alpha 3} &= \mathrm{c}_{3i}u_{i,\alpha} + \mathrm{c}_{\alpha i}w_i + u_{i,\alpha}w_i\,, \\ \mathrm{C}_{3\alpha} &= \mathrm{C}_{\alpha 3}\,, \\ \mathrm{C}_{33} &= 1 + 2\mathrm{c}_{3i}w_i + w_i w_i\,, \\ \mathrm{K}_{\alpha\beta} &= \mathrm{B}_{\alpha\beta} + \mathrm{c}_{3i,\alpha}u_{i,\beta} + \mathrm{c}_{3i,\beta}u_{i,\alpha} + \mathrm{c}_{\alpha i}w_{i,\beta} \\ &\qquad + \mathrm{c}_{\beta i}w_{i,\alpha} + u_{i,\alpha}w_{i,\beta} + u_{i,\beta}w_{i,\alpha}\,, \\ \mathrm{K}_{\alpha 3} &= (\mathrm{c}_{3i,\alpha}w_i + \mathrm{c}_{3i}w_{i,\alpha} + w_i w_{i,\alpha}) + 2\chi(\mathrm{c}_{\alpha i}w_i + \mathrm{c}_{3i}u_{i,\alpha} + w_i u_{i,\alpha}), \\ \mathrm{K}_{3\alpha} &= \mathrm{K}_{\alpha 3}\,, \\ \mathrm{K}_{33} &= 4\chi(1 + 2\mathrm{c}_{3i}w_i + w_i w_i). \end{aligned} \tag{4.18}$$

Equations (4.18) are in fact quite compact expressions, well suited for a numerical implementation.

4.3. The principle of virtual work

Let $\mathbf{S}$ be the second Piola–Kirchhoff stress tensor of the shell space.

The principle of virtual displacement in three-dimensions reads

$$\int_{\mathcal{B}} \frac{1}{2}\mathbf{S} : \delta\mathbf{C}\, dV - \int_{\mathcal{B}} \boldsymbol{f}\cdot\delta\boldsymbol{x}\, dV - \int_{\partial\mathcal{B}_t} \boldsymbol{t}\cdot\delta\boldsymbol{x}\, dS = 0, \tag{4.19}$$

where $\boldsymbol{f}$, $\boldsymbol{t}$ are the body and the surface forces, respectively, $dV = M\, d\sigma\, dz$ (see Naghdi [1]) and $d\sigma$ is a surface element of the shell midsurface given by $d\sigma = \sqrt{A}\, d\vartheta^1\, d\vartheta^2$, $A = \det(A_{\alpha\beta})$. Tractions are prescribed on the part $\partial\mathcal{B}_t$ of the boundary $\partial\mathcal{B}$ ($\partial\mathcal{B}_t \subset \partial\mathcal{B}$). We further assume that the shell midsurface $\mathcal{M}$ has a smooth curve $\partial\mathcal{M}$ as boundary with the length parameter s. The boundary of the shell consists of three parts: an upper, a lower, and a lateral surface. If we denote the upper surface by $\partial\mathcal{B}^+$, the lower one by $\partial\mathcal{B}^-$ and the lateral one by $\partial\mathcal{B}^s$ and make use of the notation $M^+ = M|_{z=h/2}$, $M^- = M|_{z=-h/2}$, and M^s for M at the lateral surface, we may write for the surface elements $dS^+ = M^+ d\sigma$, $dS^- = M^- d\sigma$ and $dS^s = M^s\, dz\, ds$.

We first consider the external virtual work.

$$\delta\mathcal{W}_{\text{ext}} := \int_{\mathcal{B}} \boldsymbol{f}\cdot\delta\boldsymbol{x}\, dV + \int_{\partial\mathcal{B}} \boldsymbol{t}\cdot\delta\boldsymbol{x}\, dS. \tag{4.20}$$

With the definitions

$$\begin{aligned}
\boldsymbol{p} &:= \int_{-h/2}^{h/2} \boldsymbol{f} M\, dz + M^+\mathbf{t}^+ + M^-\mathbf{t}^-,\\
\boldsymbol{l} &:= \int_{-h/2}^{h/2} z\boldsymbol{f} M\, dz + \frac{h}{2}M^+\boldsymbol{t}^+ - \frac{h}{2}M^-\boldsymbol{t}^-,\\
\boldsymbol{q} &:= \int_{-h/2}^{h/2} z^2\boldsymbol{f} M\, dz + \frac{h^2}{4}M^+\boldsymbol{t}^+ + \frac{h^2}{4}M^-\boldsymbol{t}^-,\\
\boldsymbol{p}^s &:= \int_{-h/2}^{h/2} \boldsymbol{t}^s M^s\, dz\,,\\
\boldsymbol{l}^s &:= \int_{-h/2}^{h/2} z\boldsymbol{t}^s M^s\, dz\,,\\
\boldsymbol{q}^s &:= \int_{-h/2}^{h/2} z^2\boldsymbol{t}^s M^s\, dz\,,
\end{aligned} \tag{4.21}$$

Equation (4.20) reduces to

$$\delta \mathcal{W}_{\text{ext}} = \int_{\mathcal{M}} \left[\boldsymbol{p} \cdot \delta \boldsymbol{x}^0 + (\boldsymbol{l} + \chi \boldsymbol{q}) \cdot \delta \boldsymbol{a}_3 + (\boldsymbol{q} \cdot \boldsymbol{a}_3) \delta \chi \right] d\sigma + \int_{\partial \mathcal{M}_t} \left[\boldsymbol{p}^s \cdot \delta \boldsymbol{x}^0 + (\boldsymbol{l}^s + \chi \boldsymbol{q}^s) \cdot \delta \boldsymbol{a}_3 + (\boldsymbol{q}^s \cdot \boldsymbol{a}_3) \delta \chi \right] ds \tag{4.22}$$

as the two-dimensional form of the external power. In (4.22) it is presupposed that on the entire upper and lower surfaces tractions are prescribed. However, we assume that only on a part $\partial \mathcal{M}_t$ of the boundary $\partial \mathcal{M}$ of the SMS tractions are prescribed.

To consider the internal virtual power we notice first that it is more appropriate to make use of the relation

$$\mathbf{S} = \mathbf{C}^{-1} \boldsymbol{\Xi} \tag{4.23}$$

since the inelastic constitutive model, as shown in Sec. 3.2.1, is formulated in terms of $\boldsymbol{\Xi}$. We define first the pull-back of $\mathbf{S}$ under $\mathbf{M}$ which gives a stress tensor defined with respect to the midsurface

$$\mathbf{S}^0 = \mathbf{M}^{-1} \mathbf{C}^{-1} \boldsymbol{\Xi} \mathbf{M}^{-\mathrm{T}}. \tag{4.24}$$

REMARK 5. Note that $\mathbf{S}^0$ still depends on the normal coordinate z. □

Equations (3.25), (4.23) and (4.24) motivate the following definitions

$$\begin{aligned} \mathbf{n} &:= \int_{-h/2}^{+h/2} \frac{1}{2} \mathbf{S}^0 N \, dz = \int_{-h/2}^{+h/2} \mathbf{M}^{-1} \mathbf{C}^{-1} \frac{\partial \psi}{\partial \overline{\boldsymbol{\alpha}}} \mathbf{M}^{-\mathrm{T}} M \, dz, \\ \mathbf{m} &:= \int_{-h/2}^{+h/2} z \mathbf{M}^{-1} \mathbf{C}^{-1} \frac{\partial \psi}{\partial \overline{\boldsymbol{\alpha}}} \mathbf{M}^{-\mathrm{T}} M \, dz \end{aligned} \tag{4.25}$$

with the help of which as well as with (4.22), the principle of virtual work given in (4.19) takes the form

$$\int_{\mathcal{M}} \left[\mathbf{n} : \delta \mathbf{C}^0 + \mathbf{m} : \delta \mathbf{K} \right] d\sigma - \int_{\mathcal{M}} \left[\boldsymbol{p} \cdot \delta \boldsymbol{x}^0 + (\boldsymbol{l} + \chi \boldsymbol{q}) \cdot \delta \boldsymbol{a}_3 + (\boldsymbol{q} \cdot \boldsymbol{a}_3) \delta \chi \right] d\sigma - \int_{\partial \mathcal{M}} \left[\boldsymbol{p}^s \cdot \delta \boldsymbol{x}^0 + (\boldsymbol{l}^s + \chi \boldsymbol{q}^s) \cdot \delta \boldsymbol{a}_3 + (\boldsymbol{q}^s \cdot \boldsymbol{a}_3) \delta \chi \right] ds = 0. \tag{4.26}$$

For given external forces, the integrals (4.21) can be expressed in almost closed form. For very thin shells the terms $\chi \boldsymbol{q} \cdot \delta \boldsymbol{a}_3$, $\boldsymbol{q} \cdot \boldsymbol{a}_3 \delta \chi$ in (4.26) can be neglected as being of higher order. However, in order to allow for the use of complex constitutive laws and path-dependent behaviour (e.g. cyclic loading), the evaluation of (4.25) is carried out in practical computations numerically. That is, the constitutive equations are considered pointwise over the shell thickness.

4.4. Numerical implementation

In this section computational issues in conjunction with a possible finite element formulation are discussed. The time integration procedure of the constitutive model at hand is outlined and necessary operations of local iterations are discussed. A closed form of the algorithmic tangent operator is presented.

4.4.1. Time integration and local iterations. We consider two consecutive times t_n and t_{n+1} with time increment $\Delta t = t_{n+1} - t_n$. Since the unimodular tensor $\mathbf{F}_p$ is an element of the Lie group $SL^+(3,\mathbb{R})$ and the tensor $\mathbf{L}_p$ is an element of the corresponding Lie algebra, the exponential map can be used for time integration. Therefore, the following update formula is considered

$$\mathbf{F}_p|_{n+1} = \mathbf{F}_p|_n \exp[\Delta t \mathbf{L}_p] \tag{4.27}$$

for some $\mathbf{L}_p$ in the interval Δt, the choice of which is defined by means of the integration procedure. This algorithm preserves the condition of plastic incompressibility exactly. From (4.27) follows directly the update formula for the elastic strain measure (3.26)

$$\mathbf{C}\,\mathbf{C}_p^{-1}|_{n+1} = \mathbf{C}|_{n+1} \exp(-\Delta t \mathbf{L}_p)\mathbf{C}_p{}^{-1}|_n \exp(-\Delta t \mathbf{L}_p^T). \tag{4.28}$$

Due to (3.30) we update the tensor $\mathbf{L}_p$ as

$$\mathbf{L}_p = \dot{\phi}\,\boldsymbol{\nu}^T. \tag{4.29}$$

Since isotropy was assumed in Sec. 3.2.2, the tensors $\boldsymbol{\Xi}$ and $\overline{\boldsymbol{\alpha}}^T$ or $\boldsymbol{\Xi}$ and $\mathbf{C}\,\mathbf{C}_p{}^{-1}$ are coaxial. Thus the single terms in (4.28) can be rearranged and the logarithms can be taken to give [45]

$$\begin{aligned} \ln(\mathbf{C}\,\mathbf{C}_p{}^{-1})_{n+1} &= \ln\left[\mathbf{C}_{n+1}\mathbf{C}_p{}^{-1}|_n \exp(-2\Delta t \mathbf{L}_p^T)\right], \\ \overline{\boldsymbol{\alpha}}_{n+1}^T &= (\overline{\boldsymbol{\alpha}}^{\text{trial}})^T - 2\Delta t \mathbf{L}_p^T, \\ (\overline{\boldsymbol{\alpha}}^{\text{trial}})^T &= \ln \mathbf{C}_{n+1}\mathbf{C}_p{}^{-1}|_n . \end{aligned} \tag{4.30}$$

Next, we give the update of the stress tensor as, where (3.27) is considered for the definition of the trial stress

$$\begin{aligned} \boldsymbol{\Xi}_{n+1} &= \boldsymbol{\Xi}^{\text{trial}} - \mu 2\Delta t \mathbf{L}_p^T, \\ &= \boldsymbol{\Xi}^{\text{trial}} - 2\Delta t \dot{\phi} \mu \boldsymbol{\nu}_{n+1}, \end{aligned} \tag{4.31}$$

$$\boldsymbol{\Xi}^{\text{trial}} := K \operatorname{tr}(\overline{\boldsymbol{\alpha}}^{\text{trial}})^T \mathbf{I} + \mu \left((\overline{\boldsymbol{\alpha}}^{\text{trial}})^T - \frac{1}{3}\operatorname{tr}(\overline{\boldsymbol{\alpha}}^{\text{trial}})^T \right) \tag{4.32}$$

for some $\dot{\phi}$ in the corresponding interval.

From $(3.31)_2$ and (4.31) follows

$$\Pi_{n+1} = \Pi^{\text{trial}} - 3\Delta t \mu \dot{\phi}. \tag{4.33}$$

We are now looking for the determination of $\dot{\phi}$ in accordance with (2.23) to $(2.19)_3$ as well as with (4.33). We adopt the mid-point rule according to which we have

$$\Pi = \frac{1}{2}(\Pi_{n+1} + \Pi_n) = \frac{1}{2}(\Pi^{\text{trial}} - 3\Delta t \mu \dot{\phi} + \Pi_n); \tag{4.34}$$

$$\begin{aligned} \dot{Z} &= \frac{Z_{n+1} - Z_n}{\Delta t}, \\ Z &= \frac{1}{2}(Z_{n+1} + Z_n). \end{aligned} \tag{4.35}$$

We insert Eqs. (4.35) into (2.23) and $(3.31)_2$ to obtain an explicit equation for the determination of the internal variable Z

$$Z = \frac{m\Delta t \Pi \dot{\phi} Z_1 + 2Z_0 Z_n}{m\Delta t \Pi \dot{\phi} + 2Z_0}, \tag{4.36}$$

which depends explicitly on $\dot{\phi}$. Inserting (4.36) into $(3.31)_3$ yields a nonlinear equation for the determination of $\dot{\phi}$

$$\dot{\phi} = \frac{2}{\sqrt{3}} D_0 \exp\left[-\frac{1}{2}\frac{N+1}{N}\left(\frac{Z(\Pi, \dot{\phi})}{\Pi}\right)^{2N}\right], \tag{4.37}$$

where Π is computed by means of (4.33). Equation (4.37) has to be solved iteratively by Newton's method.

4.4.2. The algorithmic tangent operator. The algorithmic tangent operator is obtained as the linearization of the update formula for the second Piola–Kirchhoff tensor $\mathbf{S}$ with respect to the right Cauchy–Green deformation tensor. With (4.31) we obtain

$$\mathbf{S} = \mathbf{C}^{-1}(\boldsymbol{\Xi}^{\text{trial}} - 2\Delta t \dot{\phi} \mu \boldsymbol{\nu}). \tag{4.38}$$

The derivative with respect to $\mathbf{C}$ gives

$$\begin{aligned} \frac{\partial \mathbf{S}}{\partial \mathbf{C}} = {} & \frac{\partial \mathbf{C}^{-1}}{\partial \mathbf{C}}(\boldsymbol{\Xi}^{\text{trial}} - 2\Delta t \dot{\phi} \mu \boldsymbol{\nu}) + \mathbf{C}^{-1} \frac{\partial \boldsymbol{\Xi}^{\text{trial}}}{\partial \mathbf{C}} \\ & - 2\Delta t \mu \frac{\partial \dot{\phi}}{\partial \Pi^{\text{trial}}} \frac{\partial \Pi^{\text{trial}}}{\partial \boldsymbol{\Xi}^{\text{trial}}} \frac{\partial \boldsymbol{\Xi}^{\text{trial}}}{\partial \mathbf{C}} \mathbf{C}^{-1} \boldsymbol{\nu} - 2\Delta t \mu \dot{\phi} \mathbf{C}^{-1} \frac{\partial \boldsymbol{\nu}}{\partial \boldsymbol{\Xi}^{\text{trial}}} \frac{\partial \boldsymbol{\Xi}^{\text{trial}}}{\partial \mathbf{C}}. \end{aligned} \tag{4.39}$$

The tedious algebra given in [45] leads to the very compact and closed form

$$\frac{\partial(\mathbf{S})_{ij}}{\partial(\mathbf{C})_{rs}} = -(\mathbf{C}^{-1})^{ir}(\mathbf{C}^{-1})^{sk}[(\Xi^{\text{trial}})_k{}^j - 2\Delta t\dot{\phi}\mu(\boldsymbol{\nu})_k{}^j] + \beta_1(\mathbf{C}^{-1})^{ij}(\mathbf{C}^{-1})^{rs} + \beta_2(\mathbf{C}^{-1})^{is}(\mathbf{C}^{-1})^{rj} + \beta_3(\mathbf{C}^{-1})^{ik}(\boldsymbol{\nu})_k{}^j(\mathbf{C}^{-1})^{rt}(\boldsymbol{\nu})_t{}^s, \tag{4.40}$$

where we have introduced the following notation

$$\beta_1 = K - \frac{1}{3}\mu + \Delta t\mu^2\frac{\dot{\phi}}{\Pi_{n+1}}, \qquad \beta_2 = \mu - 3\Delta t\mu^2\frac{\dot{\phi}}{\Pi_{n+1}}, \qquad \beta_3 = -2\Delta t\mu^2\left(\frac{\partial\dot{\phi}}{\partial\Pi^{\text{trial}}} - \frac{\dot{\phi}}{\Pi_{n+1}}\right). \tag{4.41}$$

In $(4.41)_3$

$$\frac{\partial\dot{\phi}}{\partial\Pi^{\text{trial}}} = \frac{\dfrac{\partial\dot{\phi}}{\partial\Pi}\dfrac{\partial\Pi}{\partial\Pi^{\text{trial}}} + \dfrac{\partial\dot{\phi}}{\partial Z}\dfrac{\partial Z}{\partial\Pi^{\text{trial}}}}{1 - \dfrac{\partial\dot{\phi}}{\partial\Pi}\dfrac{\partial\Pi}{\partial\dot{\phi}} - \dfrac{\partial\dot{\phi}}{\partial Z}\dfrac{\partial Z}{\partial\dot{\phi}}} \tag{4.42}$$

has to be considered.

4.5. Finite element formulation

We briefly discuss the interpolation of the shell geometry and then present an enhanced strain element.

4.5.1. Interpolation of shell geometry. The geometric quantities describing the shell surface (the fields $B_{\alpha\beta}$, $c_{\alpha i}$, c_{3i}, $\sqrt{A}$) are taken exactly at every integration point. The natural coordinates ϑ^α describing the shell surface are mapped onto the bi-unit square using bilinear interpolations.

On the other hand, the Cartesian components of the kinematical fields $\boldsymbol{u}$, $\boldsymbol{w}$ as well as χ are interpolated using the bilinear interpolation functions.

4.5.2. An enhanced strain functional. We formulate first a strain-based element. We appeal to the enhanced strain concept in the spirit of SIMO and RIFAI [46] applied by them to linear problems. Accordingly, the right Cauchy–Green deformation tensor itself is enhanced. This is in contrast with the nonlinear version of the concept given by SIMO and ARMERO [47] where the deformation gradient was enhanced. Accordingly, we consider the following functional

$$\frac{1}{2}\int_{\mathcal{B}}(\mathbf{C} + \mathbf{C}^i)^{-1}\Xi : \delta(\mathbf{C} + \mathbf{C}^i)\,dV - \int_{\mathcal{B}}\boldsymbol{f}\cdot\delta\boldsymbol{x}\,dV - \int_{\partial\mathcal{B}}\boldsymbol{f}\cdot\delta\boldsymbol{x}\,dS = 0, \tag{4.43}$$

where we have

$$\begin{aligned} \boldsymbol{\Xi} &= 2\varrho_{\text{ref}}\frac{\partial \psi}{\partial \tilde{\boldsymbol{\alpha}}} = K \operatorname{tr}\tilde{\boldsymbol{\alpha}}^{\mathrm{T}}\mathbf{I} + \mu\left(\tilde{\boldsymbol{\alpha}}^{\mathrm{T}} - \frac{1}{3}\operatorname{tr}\tilde{\boldsymbol{\alpha}}^{\mathrm{T}}\mathbf{I}\right), \\ \tilde{\boldsymbol{\alpha}} &= \ln[\mathbf{C}_{\mathrm{p}}^{-1}(\mathbf{C}+\mathbf{C}^{i})] \end{aligned} \tag{4.44}$$

and $\mathbf{C}^i$ is the enhanced strain field. Since $\mathbf{C}^i$ is assumed to be independent of the displacements, Eq. (4.43) splits into the following two equations

$$\frac{1}{2}\int_{\mathcal{B}}(\mathbf{C}+\mathbf{C}^{i})^{-1}\boldsymbol{\Xi} : \delta\mathbf{C}\, dV - \int_{\mathcal{B}} \boldsymbol{f}\cdot\delta\boldsymbol{u}\, dV - \int_{\partial\mathcal{B}_t} \boldsymbol{t}\cdot\delta\boldsymbol{u}\, dS = 0, \tag{4.45}$$

and

$$\frac{1}{2}\int_{\mathcal{B}}(\mathbf{C}+\mathbf{C}^{i})^{-1}\boldsymbol{\Xi} : \delta\mathbf{C}^{i}\, dV = 0. \tag{4.46}$$

The choice of the interpolation functions for $\mathbf{C}^i$ is crucial in order to arrive at well behaving elements. Equation (4.15) motivates to restrict the incompatible deformation tensor $\mathbf{C}^i$ to the form $\mathbf{C}^i = \mathbf{M}^{-\mathrm{T}}\mathbf{C}^{0^i}\mathbf{M}^{-1}$ where $\mathbf{C}^{0^i}$ is independent of z. This is equivalent to an enhancement of the strains related to the shell midsurface alone.

Equations (4.45) and (4.46) are still defined for the three-dimensional shell body. The reduction to two dimensions is carried out in the same way as demonstrated in Sec. 4.3 (compare (4.21)). One has

$$\begin{aligned} &\int_{\mathcal{M}}(\mathbf{n} : \delta\mathbf{C}^0 + m : \delta\mathbf{K})\, d\sigma - \int_{\mathcal{M}}\left[\boldsymbol{p}\cdot\delta\boldsymbol{x}^0 + (\boldsymbol{l}+\chi\boldsymbol{q})\cdot\delta\mathbf{a}_3(\boldsymbol{q}\cdot\mathbf{a}_3)\delta\chi\right] d\sigma \\ &\qquad - \int_{\partial\mathcal{M}_t}\left[\boldsymbol{p}^{\mathrm{s}}\cdot\delta\boldsymbol{x}^0 + (\boldsymbol{l}^{\mathrm{s}}+\chi\boldsymbol{q}^{\mathrm{s}})\cdot\delta 3 + (\boldsymbol{q}^{\mathrm{s}}\cdot 3)\delta\chi\right] ds = 0, \\ &\int_{\mathcal{M}}\mathbf{n} : \delta\mathbf{C}^{0^i} d\sigma = 0. \end{aligned} \tag{4.47}$$

The contributions of the external loads are defined in (4.21) while $\mathbf{n}$, $\mathbf{m}$ are now defined according to

$$\begin{aligned} \mathbf{n} &:= \int_{-h/2}^{+h/2}\mathbf{M}^{-1}\left(\mathbf{C}+\mathbf{C}^{i}\right)^{-1}\frac{\partial\psi}{\partial\tilde{\boldsymbol{\alpha}}}\mathbf{M}^{-\mathrm{T}} M\, dz, \\ \mathbf{m} &:= \int_{-h/2}^{+h/2} z\mathbf{M}^{-1}\left(\mathbf{C}+\mathbf{C}^{i}\right)^{-1}\frac{\partial\psi}{\partial\tilde{\boldsymbol{\alpha}}}\mathbf{M}^{-\mathrm{T}} M\, dz. \end{aligned} \tag{4.48}$$

The interpolation functions for the components of the incompatible deformation $\mathbf{C}^{0^i}$ are taken to be of the form

$$
\begin{aligned}
C^{0^i}_{11}(\xi,\eta) &= C_1\xi + C_2\xi\eta\,,\\
C^{0^i}_{22}(\xi,\eta) &= C_3\eta + C_4\xi\eta\,,\\
C^{0^i}_{33}(\xi,\eta) &= C_5\xi + C_6\eta + C_7\xi\eta\,,\\
C^{0^i}_{12}(\xi,\eta) &= C_8\xi + C_9\eta + C_{10}\xi\eta\,,\\
C^{0^i}_{13}(\xi,\eta) &= C_{11}\xi + C_{12}\xi\eta\,,\\
C^{0^i}_{23}(\xi,\eta) &= C_{13}\eta + C_{14}\xi\eta\,.
\end{aligned}
\tag{4.49}
$$

The quantities ξ and η are the local coordinates at the element level. Clearly, the fields $C^{0^i}_{11}\ldots C^{0^i}_{23}$ are the components of the incompatible deformation tensor $\mathbf{C}^{0^i}$ with respect to the natural curvilinear base system G_i.

The introduction of interpolation functions of the displacement fields as well as of the enhanced strain fields in (4.47) leads to two coupled nonlinear sets of algebraic equations. The enhanced strain field is assumed to be discontinuous over elements and is eliminated at the element level.

Again (4.48) have to be linearized (compare Sec. 4.4.2). The tangent operator for the shell space given by (4.40) is a fourth order tensor which we denote by $\mathbf{H}$. The systematic linearization of (4.48) leads to the following expressions

$$
\begin{aligned}
\int_{\mathcal{M}} [\Delta\mathbf{n} : \delta\mathbf{C}^0 + \Delta\mathbf{m} : \delta\mathbf{K}]\, d\sigma = \int_{\mathcal{M}} \Big(&\mathbf{H}^0(\Delta\mathbf{C}^0 + \Delta\mathbf{C}^{0^i}) + \mathbf{H}^1\Delta\mathbf{K} : \delta\mathbf{C}^0\\
&+ [\mathbf{H}^1\Delta(\mathbf{C}^0 + \mathbf{C}^{0^i}) + \mathbf{H}^2\Delta\mathbf{K}] : \delta\mathbf{K}\Big)\, d\sigma\,,\\
\int_{\mathcal{M}} \Delta\mathbf{n} : \delta\mathbf{C}^{0^i}\, d\sigma = \int_{\mathcal{M}} \Big([\mathbf{H}^0(\Delta\mathbf{C}^0 + \Delta\mathbf{C}^{0^i}) + \mathbf{H}^1\Delta\mathbf{K}] &: \delta\mathbf{C}^{0^i}\Big)\, d\sigma\,.
\end{aligned}
\tag{4.50}
$$

The following definitions hold

$$
\begin{aligned}
(\mathbf{H}^0)^{ijkl} &:= \int_{-h/2}^{+h/2} (\mathbf{M}^{-1})^i_a (\mathbf{M}^{-\mathrm{T}})^j_b (\mathbf{H})^{abrs} (\mathbf{M}^{-1})^k_r (\mathbf{M}^{-\mathrm{T}})^l_s\, M\, dz,\\
(\mathbf{H}^1)^{ijkl} &:= \int_{-h/2}^{+h/2} z(\mathbf{M}^{-1})^i_a (\mathbf{M}^{-\mathrm{T}})^j_b (\mathbf{H})^{abrs} (\mathbf{M}^{-1})^k_r (\mathbf{M}^{-\mathrm{T}})^l_s\, M\, dz,\\
(\mathbf{H}^2)^{ijkl} &:= \int_{-h/2}^{+h/2} z^2(\mathbf{M}^{-1})^i_a (\mathbf{M}^{-\mathrm{T}})^j_b (\mathbf{H})^{abrs} (\mathbf{M}^{-1})^k_r (\mathbf{M}^{-\mathrm{T}})^l_s\, M\, dz.
\end{aligned}
\tag{4.51}
$$

The integrals in (4.51) must be evaluated numerically. Further details of the implementation are standard and hence they have been omitted.

4.6. Numerical results

4.6.1. Comparison with experiments. In the first example the verification of the model presented in the previous sections is compared with experiments.

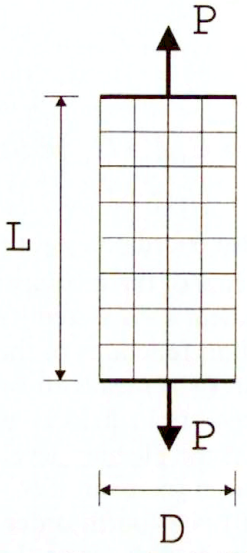

$L = 52$
$D = 8$

FIG. 5. Specimen under tension. Definition of the problem.

In [17] a specimen of pure titanium of 1 mm thickness, 8 mm width and 52 mm length (Fig. 5) was subject to different straining histories. BODNER and PARTOM used in [17] a model based on an additive decomposition of the deformation rate. The process of adjusting the calculated stress-strain curves to the experimental ones led in [17] to the following material parameters:

$$
\begin{aligned}
K &= 1.845 \times 10^5 \ \mathrm{N/mm^2}, \\
\mu &= 4.4 \times 10^4 \ \mathrm{N/mm^2}, \\
Z_0 &= 1150 \ \mathrm{N/mm^2}, \\
Z_1 &= 1400 \ \mathrm{N/mm^2}, \\
D_0 &= 10000 \ 1/\mathrm{sec}, \\
N &= 1, \\
M &= 100.
\end{aligned}
\tag{4.52}
$$

Two loading velocities corresponding to a crosshead velocity of 5 mm/min and 10 mm/min have been calculated with the model presented in this paper. It is interesting to note that a material parameter Z_1 different than that calculated by Bodner and Partom was needed to fit the experimental results.

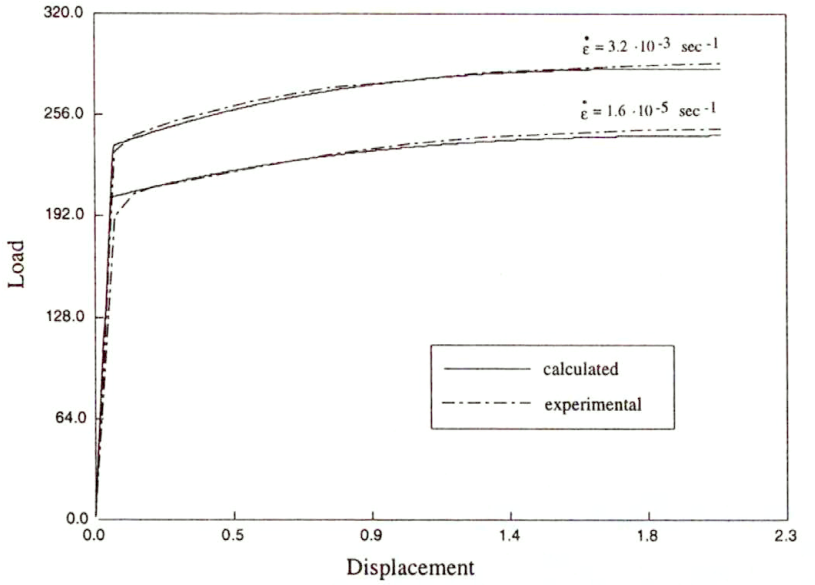

FIG. 6. Specimen under tension. Load-displacement curves.

In Fig. 6 the experimental results are compared with the calculated ones using a time step of 0.5 sec for a material parameter $Z_1 = 1540\,\mathrm{N/mm^2}$, where very good agreement can be observed.

4.6.2. Square plate under uniform loading. In all following examples the material data as formulated in (4.52) are used. A square plate is uniformly loaded as shown in Fig. 7.

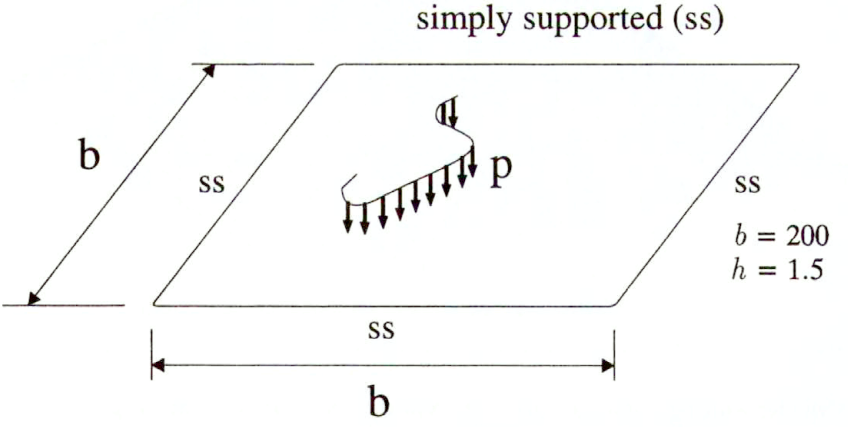

FIG. 7. Plate under dead load. Definition of the problem.

Due to symmetry conditions, only one quarter of the plate is discretized using 32×32 elements. The load is increased so as to result in a deformation velocity at

the midpoint of 1 cm/sec. Using a time step of 0.5 sec, altogether 30 time steps are calculated when the maximal loading capacity of the plate is arrived. The response of the plate is presented in Fig. 8 where the load versus the midpoint-diplacement is plotted. The maximal deformed configuration is given in Fig. 9.

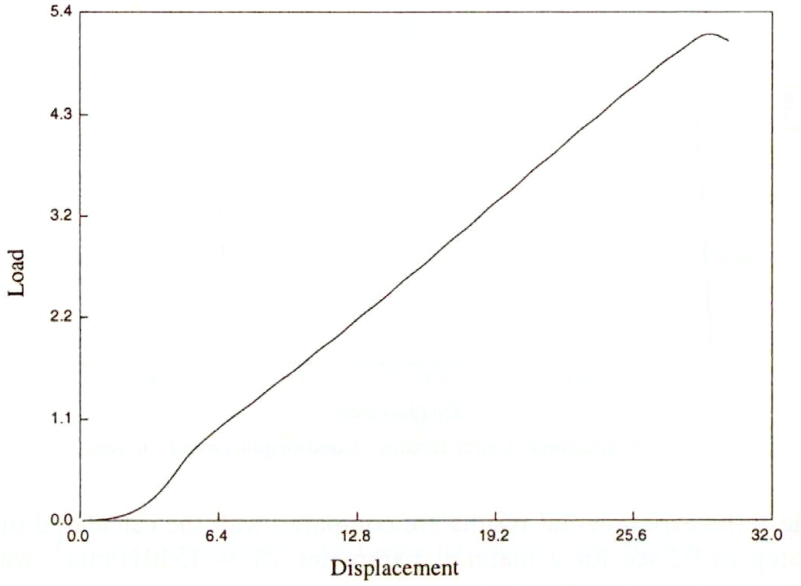

FIG. 8. Plate under dead load. Load-midpoint displacement curve.

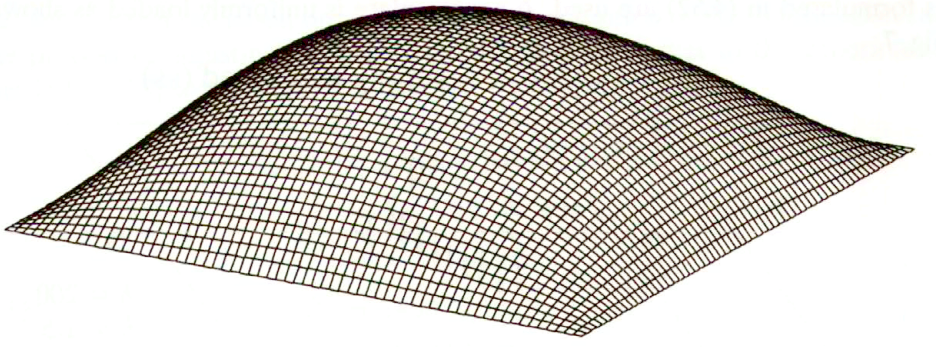

FIG. 9. Plate under dead load. Deformed configuration.

4.6.3. Cylinder with rigid diaphragms. A cylinder with rigid diaphragms is subject to a line load as described in Fig. 10. The length of the load segment is 88.35 cm. Only one eighth of the cylinder in modeled using 32×32 elements.

A loading cycle was calculated using a time step of 0.5 sec where altogether 150 time steps are considered. The loading history is chosen so as to result

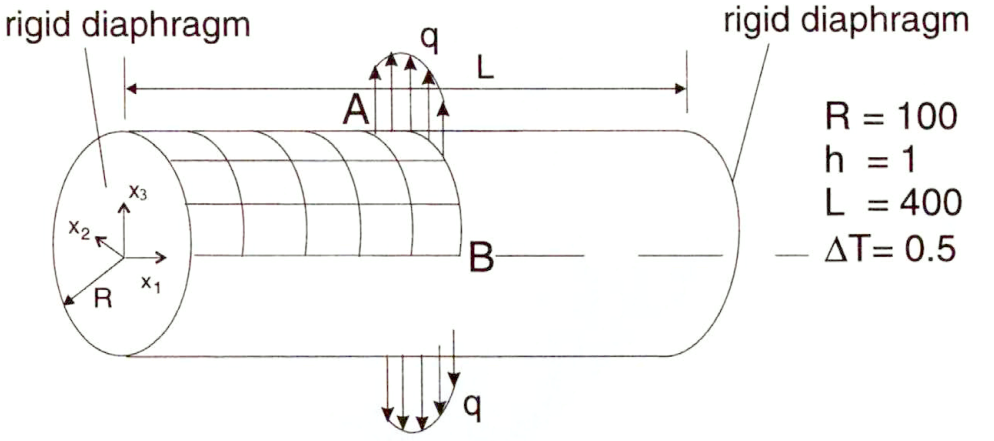

FIG. 10. Pinched cylinder with rigid diaphragm. Definition of the problem.

in a linear increase of the displacement at the top of 0.25 mm/sec. In Fig. 11 load-displacement curves are plotted for the point at the top as well as that at the side. A configuration of the cylinder at the maximal deformation is given in Fig. 12.

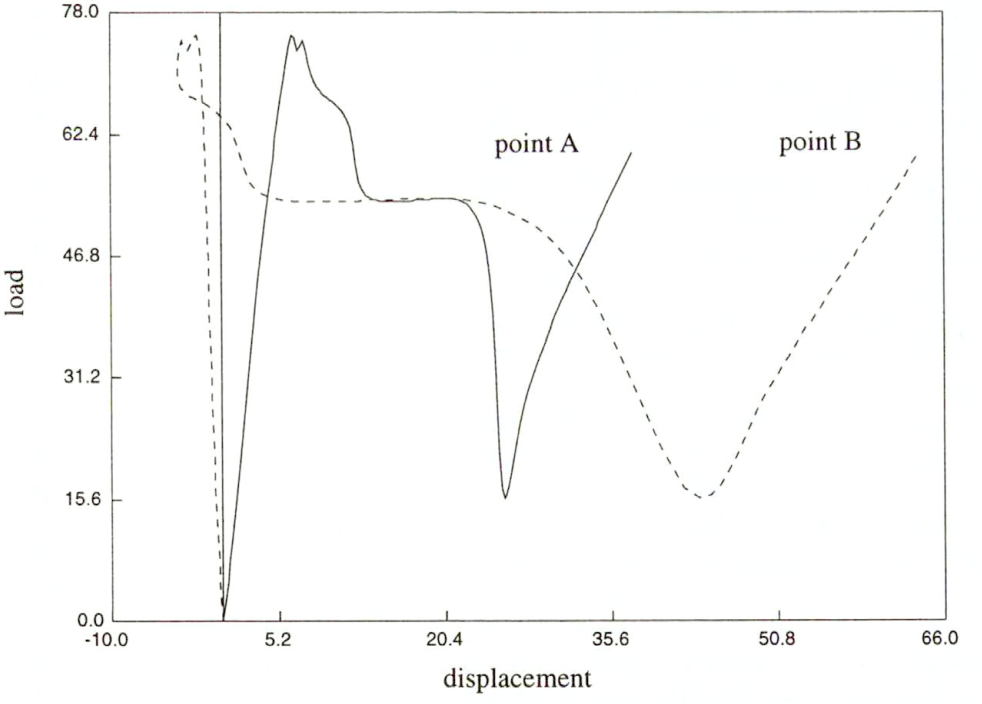

FIG. 11. Pinched cylinder with rigid diaphragm. Load-displacement curves.

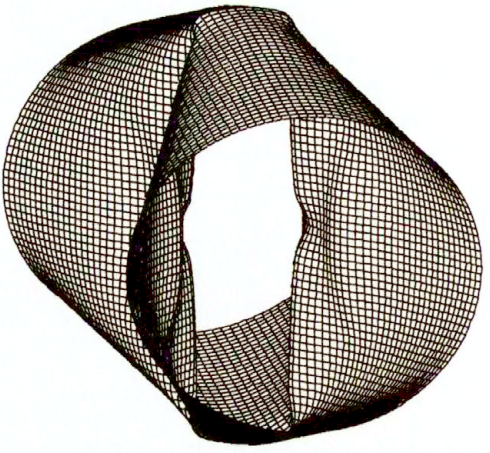

FIG. 12. Pinched cylinder with rigid diaphragm. Deformed configuration.

5. Conclusions

In this paper we give a thorough overview on the theory and numerical analysis of viscoplastic shells. In Sec. 2 we present a general theory for geometrically linear elasto-viscoplastic shells [8]. This theory is based on a two-field variational [9] principle which contains velocities and strain rates as variables to be varied independently. Families of mixed and hybrid strain elements are derived for axisymmetric shells. It is crucial to choose stable approximation schemes for the velocity and the strain rate field, respectively. Numerical experiments [12] for elastic shells demonstrate that the mixed elements are locking free and exhibit the same order of convergence for displacements and stress-like quantities such as e.g. membrane forces and bending moments. Some numerical results are presented for a cylindrical shell under internal pressure, where the viscoplastic constitutive model of BODNER and PARTOM [17] has been used.

In the major part of this paper (compare Sec. 3 and Sec. 4) we present a general theory of viscoplastic shells under finite deformation and its numerical implemetation by means of the FEM. For this purpose we first develop a general theory of finitely deformed elasto-viscoplastic three-dimensional bodies. We assume a hyperelastic model and based on the assumption of persisting isotropy, we derive a very concise representation of the elastic part of the constitutive model by introducing a logarithmic strain measure. Next, a shell theory with seven parameters is formulated, which can account for distributions of the transverse strains over the shell thickness varying linearly with the normal coordinate. Therefore, this shell model enables the use of fully three-dimensional constitutive models without using the typical "shell assumptions". Basing on the principle of virtual work, we formulate our shell equations. Furthermore, we discuss such

computional issues as time integration and the computation of the algorithmic tangent operator. Finally, an enhanced strain finite shell element is derived. Some test examples are presented.

References

1. P.M. NAGHDI, *Theory of plates and shells*, [in:] Handbuch der Physik, S. FLÜGGE and C. TRUESDELL [Eds.], Vol. VIa/2., pp. 473–479, Springer, Berlin, Heidelberg, New York 1972.
2. R. VALID, *The nonlinear theory of shells through variational principles*, John Wiley & Sons, Chichester, New York, Brisbane, Singapore 1995.
3. M. BERNADOU, *Finite element analysis for thin shells*, John Wiley & Sons, Chichester, New York, Brisbane, Singapore 1996.
4. I. CORMEAU, *Elastoplastic thick shell analysis by viscoplastic solid finite elements*, Int. J. Num. Meth. Engng., **12**, 203–227, 1978.
5. T.J.R. HUGHES and W.K. LIU, *Nonlinear finite element analysis of shells. Part 1. Three-dimensional shells*, Comp. Meth. Appl. Mech.Engng., **26**, 333–362, 1981.
6. T.J.R. HUGHES and W.K. LIU, *Nonlinear finite element analysis of shells. Part 2. Two-dimensional shells*, Comp. Meth. Appl. Mech. Engng., **27**, 167–181, 1981.
7. H. PARISCH, *Large displacements of shells including material nonlinearities*, Comp. Meth. Appl. Mech. Engng., **27**, 183–204, 1981.
8. F.G. KOLLMANN and S. MUKHERJEE, *A general, geometrically linear theory of inelastic thin shells*, Acta Mech., **57**, 41–67, 1985.
9. S. MUKHERJEE and F.G. KOLLMANN, *A new rate principle suitable for analysis of inelastic deformation of plates and shells*, J. Appl. Mech., **52**, 533–535, 1985.
10. J.T. ODEN and J.N. REDDY, *On dual complementary variational principles in mathematical physics*, Int. J. Engng. Sci., **12**, 1–29, 1974.
11. F.G. KOLLMANN and V. BERGMANN, *Numerical analysis of viscoplastic axisymmetric shells based on a hybrid strain finite element*, Comp. Mech., 7, 89–105, 1990.
12. F.G. KOLLMANN, D. CORDTS and H.-P. HACKENBERG, *Implementation and numerical tests of a family of mixed finite elements for the computation of axisymmetric viscoplastic shells*, Unpublished report MuM-Report 90/1, Technische Hochschule Darmstadt, Darmstadt, Federal Republic of Germany 1990.
13. M. KLEIBER and F.G. KOLLMANN, *A theory of viscoplastic shells including damage*, Arch. Mech., **45**, 423–437, 1993.
14. A.L. GURSON, *Continuum theory of ductile rupture by void nucleation and growth. Part 1. Yield criteria and flow rules for ductile materials*, Trans. ASME, J. Engng. Mat. Tech., **99**, 2–15, 1977.
15. Q. AN and F.G. KOLLMANN, *A general theory of finite deformation of viscoplastic thin shells*, Acta Mech., **117**, 47–70, 1996.
16. P. PERZYNA, *Fundamental problems in viscoplasticity*, [in:] Advances in Applied Mechanics, G.G. CHERNYI *et al.* [Eds], pp. 243–377, Academic Press, 1966.
17. S.R. BODNER and Y. PARTOM, *Constitutive equations for elastic-viscoplastic strain-hardening materials*, ASME, J. Appl. Mech., **42**, 385–389, 1975.
18. J.L. CHABOCHE, *Constitutive equations for cyclic plasticity and cyclic viscoplasticity*, Int. J. Plasticity, **5**, 247–302, 1989.
19. E. KREMPL, J. MCMAHON and D. YAO, *Viscoplasticity based on overstress with a differential growth law for the equilibrium stress*, Mech. of Mat., **5**, 35–48, 1986.
20. E.A. STECK, *A stochastic model for the high-temperature plasticity of metals*, Int. J. Plasticity, 1, 243–258, 1985.
21. M.B. RUBIN, *A elasto-viscoplastic model for large strains*, Int. J. Engng. Sci., **24**, 1083–1095, 1986.

22. P.M. NAGHDI and J.A. TAPP, *Restrictions on constitutive equations of finitely deformed elastic-plastic materials*, Q.J. Mech. Appl. Math., **28**, 25–46, 1975.

23. I. NISHIGUCHI, T.-L. SHAM and E. KREMPL, *A finite deformation theory of viscoplasticity based on overstress. Part I. Constitutive equations*, J. Appl. Mech., **57**, 548–552, 1988.

24. I. NISHIGUCHI, T.-L. SHAM and E. KREMPL, *A finite deformation theory of viscoplasticity based on overstress. Part II. Finite element implementation and numerical experiments*, J. Appl. Mech., **57**, 553–561, 1988.

25. A.L. ETEROVIC and K.J. BATHE, *A hyperelastic-based large strain elasto-plastic constitutive formulation with combined isotropic-kinematic hardening using the logarithmic stress and strain measures*, Int. J. Num. Meth. Engng., **30**, 1099–1115, 1990.

26. G. WEBER and L. ANAND, *Finite deformation constitutive equations and a time integration procedure for isotropic hyperelastic-viscoplastic solids*, Comp. Meth. Appl. Mech. Engng., **79**, 465–477, 1990.

27. C. MIEHE and E. STEIN, *A canonical model of multiplicative elasto-plasticity: formulation and aspects of the numerical implementation*, Eur. J. Mech., A/Solids, **11**, 25–43, 1992.

28. J.C. SIMO, *A framework for finite strain elastoplasticity based on maximum dissipation. Part II. Computational aspects*, Comp. Meth. Appl. Mech. Engng., 368, 1–31, 1988.

29. F.G. KOLLMANN and V. BERGMANN, *A new finite element for geometrically linear, inelastic analysis of axisymmetric plates and shells*, Unpublished report, Cornell University, Theoret. and Appl. Mech., Ithaca, N.Y. 1986.

30. O.C. ZIENKIEWICZ, J. BAUER, K. MORGAN and E. ONATE, *A simple and efficient element for axisymmetric shells*, Int. J. Num. Meth. Engng., **11**, 1545–1558, 1977.

31. H.-P. HACKENBERG, *Über die Anwendung inelastischer Stoffgesetze auf finite Deformationen mit der Methode der Finiten Elemente*, PhD Thesis, Technische Hochschule Darmstadt, 1991.

32. D. CORDTS and F.G. KOLLMANN, *An implicit time integration scheme for inelastic constitutive equations with internal state variables*, Int. J. Num. Meth. Engng., **23**, 533–554, 1986.

33. E. MARSDEN and T.J.R. HUGHES, *Mathematical foundations of elasticity*, Prentice Hall, Englewood Cliffs, 1983.

34. J.F. BESSELING, *A thermodynamic approach to rheology*, [in:] Irreversible Aspects of Continuum Mechanics, H. PARKUS and L.I. SEDDOV [Eds], pp. 16–53, Springer, Wien 1968.

35. E. KRÖNER, *Allgemeine Kontinuumstheorie der Versetzungen und Eigenspannungen*, Arch. Rat. Mech. Anal., **4**, 4, 273–334, 1960.

36. E.H. LEE, *Elastic-plastic deformation at finite strains*, Trans. ASME, J. Appl. Mech., **36**, 1–6, 1969.

37. C. SANSOUR and F.G. KOLLMANN, *On theory and numerics of large viscoplastic deformation*, [Prep. for press 1996].

38. J.C. SIMO and D.D. FOX, *On stress resultant geometrically exact shell model. Part I. Formulation and optimal parametrization*, Comp. Meth. Appl. Mech. Engng., **72**, 267–304, 1989.

39. Y. BASAR, Y. DING and W.B. KRAETZIG, *Finite rotation shell elements via mixed formulations*, Comp. Mech., **10**, 289–306, 1992.

40. P. WRIGGERS and F. GRUTTMANN, *Thin shell with finite rotations in Biot stresses: theory and finite element formulation*, Int. J. Num. Meth. Engng., **36**, 4027–4043, 1993.

41. A. LIBAI and J.G. SIMMONDS, *Nonlinear elastic shell theory*, [in:] Advances in Applied Mechanics, HUTCHINSON and WU [Eds.], Academic Press, New York, USA 1983.

42. J. MAKOWSKI, J. CHROSCIELEWSKI and H. STUMPF, *Genuinely resultant shell finite elements accounting for geometric and material nonlinearity*, Int. J. Num. Meth. Engng., **35**, 63–94, 1992.

43. C. SANSOUR and H. BUFLER, *An exact finite rotation shell theory, its mixed variational formulation and its finite element implementation*, Int. J. Num. Meth. Engng., **34**, 73–115, 1992.

44. C. SANSOUR and H. BEDNARCZYK, *The Cosserat surface as a shell model, theory and finite-element formulation*, Comp. Meth. Appl. Mech. Engng., **120**, 1–32, 1995.

45. C. SANSOUR and F.G. KOLLMANN, *Large viscoplastic deformations of shells. Theory and finite element formulation*, [Prep. for press 1996].

46. J.C. SIMO and M.S. RIFAI, *A class of mixed assumed strain methods and the method of incompatible modes*, Int. J. Num. Meth. Engng., **29**, 1595–1638, 1992.

47. J.C. SIMO and F. AMERO, *Geometrically nonlinear enhanced strain mixed methods and the method of incompatible modes*, Int. J. Num. Meth. Engng., **33**, 1413–1449, 1992.

TECHNISCHE HOCHSCHULE DARMSTADT
FACHGEBIET MASCHINENELEMENTE UND MASCHINENAKUSTIK
Magdalenenstr. 4, 64289 Darmstadt, Germany.

Received December 8, 1996; new version March 21, 1997.